Distinct diurnal variation of organic aerosol hygroscopicity and its relationship with oxygenated organic aerosol

Ye Kuang[1,*,†], Yao He[2,†], Wanyun Xu[5], Pusheng Zhao[6], Yafang Cheng[4], Gang Zhao[3], Jiangchuan Tao[1], Nan Ma[1], Hang Su[4], Yanyan Zhang[1], Jiayin Sun[7], Peng Cheng[7], Wenda Yang[7], Shaobin Zhang[1], Cheng Wu[7], Yele Sun[2,*], Chunsheng Zhao[3]

[1]{Institute for Environmental and Climate Research, Jinan University, Guangzhou 511443, China}

[2] {State Key Laboratory of Atmospheric Boundary Layer Physics and Atmospheric Chemistry, Institute of Atmospheric Physics, Chinese Academy of Sciences, Beijing 100029, China}

[3] {Department of Atmospheric and Oceanic Sciences, School of Physics, Peking University, Beijing, China}

[4] {Max Planck Institute for Chemistry, Mainz 55128, Germany}

[5] {State Key Laboratory of Severe Weather & Key Laboratory for Atmospheric Chemistry, Institute of Atmospheric Composition, Chinese Academy of Meteorological Sciences, Beijing 100081, China}

[6] {Institute of Urban Meteorology, China Meteorological Administration, Beijing 100089, China}

[7] {Institute of Mass Spectrometer and Atmospheric Environment, Jinan University, Guangzhou 510632, China}

† These authors contribute equally to this paper.

*Correspondence to: Ye Kuang (kuangye@jnu.edu.cn), Yele Sun (sunyele@mail.iap.ac.cn)

Abstract

The hygroscopicity of organic aerosols (OA) is important for investigation of its climatic and environmental impacts. However, the hygroscopicity parameter κ_{OA} remains poorly characterized, especially in the relatively polluted environment on the North China Plain (NCP). Here we conducted simultaneous wintertime measurements of bulk aerosol chemical compositions of $PM_{2.5}$ and PM_1, and bulk aerosol hygroscopicity of PM_{10} and PM_1 on the NCP using a capture vaporizer time-of-flight aerosol chemical speciation monitor (CV-ToF-ACSM) and a humidified nephelometer system which measures aerosol light scattering enhancement factor $f(\mathrm{RH})$. A method for calculating κ_{OA} based on $f(\mathrm{RH})$ and bulk aerosol chemical composition measurements was developed. We found that κ_{OA} varied in a wide range with significant diurnal variations. The derived κ_{OA} ranged from almost 0.0 to 0.25 with an average (±1σ) of 0.08 (±0.06) for the entire study. The derived κ_{OA} was highly correlated with f_{44} (fraction of *m/z* 44 in OA measured by CV-ToF-ACSM), an indicator of oxidation degree of OA (R=0.79), and the relationship can be parameterized as κ_{OA} =1.04 × f_{44} - 0.02 (κ_{OA}=0.3×O:C - 0.02, based on the relationship between f_{44} and O/C ratio for CV-ToF-ACSM). On average, κ_{OA} reached the minimum (0.02) in the morning near 07:30 and then increased rapidly reaching the peak value of 0.16 near 14:30. The diurnal variations of κ_{OA} were highly and positively correlated with those of mass fractions of oxygenated OA (R = 0.95), indicating that photochemical processing played a dominant role for the increase of κ_{OA} in winter on NCP. Results in this study demonstrate the potential wide applications of humidified nephelometer system together with aerosol composition measurements for investigating the hygroscopicity of OA in various environments, and highlight that the parameterization of κ_{OA} as a function of OA aging processes needs to be considered in chemical transport models for better evaluating the impacts of OA on cloud formation, atmospheric chemistry and radiative forcing.

1 Introduction

Aerosol hygroscopic growth plays significant roles in different atmospheric processes including atmospheric radiation transfer, cloud formation, visibility degradation, atmospheric multiphase chemistry and even air-pollution-related health effects, and therefore is crucial for studies on aerosol

climatic and environmental impacts. Organic materials in ambient aerosol particles, usually referred to organic aerosols (OA), contribute substantially to ambient aerosol mass and often contribute more than half to submicron aerosol particle mass under dry state (Jimenez et al., 2009). The hygroscopicity parameter κ (Petters and Kreidenweis, 2007) of organic aerosols (κ_{OA}) is a key parameter for investigating the roles of organic aerosol in radiative forcing, cloud formation and atmospheric chemistry. Liu and Wang (2010) demonstrated that 50% increases in κ of secondary organic aerosol (0.14 ± 0.07) can result in up to 40% increases in predicted cloud condensation nuclei (CCN) concentration. Rastak et al. (2017) reported that global average aerosol radiative forcing would decrease about 1 W/m^2 should κ_{OA} increase from 0.05 to 0.15, which is of the same order with the overall climate forcing of anthropogenic aerosol particles during the industrialization period. Li et al. (2019) reported that organic aerosol liquid water contributed 18-32% to total particle liquid water content in Beijing. Despite its importance, κ_{OA} has not yet been well characterized due to the extremely complex chemical compositions of organic aerosol. Therefore, it is important to conduct more researches on the spatiotemporal variation of κ_{OA} and its relationship with aerosol chemical compositions to reach a better characterization and come up with more appropriate parameterization schemes in chemical, meteorological and climate models.

The large variety in OA chemical constituents makes it difficult to directly link κ_{OA} to specific organic aerosol compositions. The OA chemical composition is tightly connected to their volatile organic precursors, which are also rich in variety and come from different natural and anthropogenic sources. OA with different oxidation levels also behave differently in respect to hygroscopic growth. Thus, studies on κ_{OA} at different locations and seasons have reported distinct characteristics. Many studies have investigated the influence of OA oxidation level (represented by O:C ratio or fraction of *m/z* 44 in OA, f_{44}, which are determined from aerosol mass spectrometer measurements) on its hygroscopicity (Chang et al., 2010;Lambe et al., 2011;Duplissy et al., 2011;Mei et al., 2013b;Wu et al., 2013;Hong et al., 2015;Chen et al., 2017;Massoli et al., 2010) and found that the average κ_{OA} generally increases as a function of organic aerosol oxidation level. However, the statistical empirical relationship between κ_{OA} and O:C ratio or f_{44} differs much among different studies. Several studies have also analyzed the diurnal variation characteristics of κ_{OA} at different locations and seasons (Cerully et al., 2015;Bougiatioti et al., 2016;Deng et al., 2018;Deng et al., 2019;Thalman et al., 2017), with some exhibiting distinct diurnal variations (Deng et al., 2018;Deng et al., 2019;Bougiatioti et al.,

2016) and others not (Cerully et al., 2015). Despite this, the studies on κ_{OA} in the relatively polluted North China Plain (NCP) region are very limited (Wu et al., 2016). The diurnal characteristics of κ_{OA} on the NCP have not been reported so far. Therefore, more investigation into the diurnal variation of κ_{OA} and its relationship with OA oxidation level is required to better understand its characteristics in the NCP.

The Humidity Tandem Differential Mobility Analyzer (HTDMA) or CCN counter has been widely used for aerosol hygroscopicity measurements. Both the HTMDA and size-resolved CCN measurements can only be used to derive a κ within a certain size range (HDTMA: usually diameter below 300 nm, with a reported highest diameter of 360 nm (Deng et al., 2019), CCN: with diameter up to ~200 nm (Zhang et al., 2014;Rose et al., 2010)). The aerosol particles contributing most to aerosol optical properties (Bergin et al., 2001;Quinn et al., 2002;Cheng et al., 2008;Ma et al., 2011;Kuang et al., 2018) and aerosol liquid water content (Bian et al., 2014) in continental regions are usually in the diameter range of 200 nm to 1μm, which the HTDMA and CCN hygroscopicity measurements cannot represent. Results from several studies have reported that κ_{OA} usually differentiates among particle size (Frosch et al., 2011;Kawana et al., 2016;Deng et al., 2019). For example, Deng et al. (2019) found that κ_{OA} increases with the increases in particle dry diameter. These results further highlight a need for characterization of κ_{OA} of larger particles.

The humidified nephelometer system which measures aerosol light scattering enhancement factors is also widely used in aerosol hygroscopicity research (Titos et al., 2016). The hygroscopicity parameter κ retrieved from measured light scattering enhancement factor is usually referred to as $\kappa_{f(\mathrm{RH})}$ (Chen et al., 2014;Kuang et al., 2017), which represents the overall hygroscopicity of aerosol particles with their diameters ranging from 200 nm to 800 nm for continental aerosols (see discussions in Sect.3.3 for physical understanding of $\kappa_{f(\mathrm{RH})}$). Using the retrieved $\kappa_{f(\mathrm{RH})}$ together with bulk aerosol chemical compositions of PM_1 (particulate matter with aerodynamic diameter less than 1 μm, corresponding to mobility diameter of approximately760 nm assuming spherical particles and a particle density of 1.7 g/cm^3), κ_{OA} can be derived, representing the hygroscopicity of organic aerosol particles in the diameter range of 200 to about 800 nm. In this study, the light scattering enhancement factors of both PM_{10} (particulate matter with aerodynamic diameter less than 10 μm) and PM_1 particles were measured at a rural site on the NCP in winter 2018, together with aerosol chemical compositions by a capture vaporizer time-of-flight aerosol chemical speciation monitor (CV-ToF-

ACSM). By integrating these two different measurements, κ_{OA} is derived, and the relationship between κ_{OA} and OA oxidation degree, as well as the diurnal variation of κ_{OA} is elucidated.

2 Site and instruments

From 11th November to 24th December 2018, continuous measurements of physical, optical and chemical properties of ambient aerosol particles as well as meteorological parameters such as temperature, wind speed and direction and relative humidity were made at the Gucheng site in Dingxing county, Hebei province, China. The sampling site, an Ecological and Agricultural Meteorology Station (39°09'N, 115°44'E) of the Chinese Academy of Meteorological Sciences, is located between Beijing (~ 100 km) and Baoding (~40 km), two large cities on the North China Plain, and is surrounded by farmland and small residential towns.

2.1 Inlet system and instruments

During this field campaign, all instruments were housed in an air-conditioned container, with the temperature held almost constant near 24 ℃. The schematic diagram of the inlet systems for the aerosol sampling instruments is displayed in Fig.1. Three inlet impactors are used for aerosol sampling, two PM_{10} inlets and one PM_1 inlet, respectively sampling ambient aerosol particles with aerodynamic diameter less than 10 μm and 1 μm. Nafion driers with lengths of 1.2 m were placed downstream of each PM impactor inlet, which can drop the RH of sampled air below 15%, thus, sampled aerosol particles can be treated as in dry state. Additionally, downstream every PM impactor inlet an MFC (mass flow controller) and a pump were added for automatic flow compensation, to ensure that each impactor reaches their required flow rate of 16.7 L/min and guaranteeing for the right cut diameters.

Aerosol sampling instruments can be categorized into four groups according to their inlet routes. The first group (group1) downstream of the first PM_{10} inlet is comprised of only one instrument, the Aerodynamic Particle Sizer (APS, TSI Inc., Model 3321), measuring the size distribution of ambient aerosol particles with aerodynamic diameter ranging from 700 nm to 20 μm at a temporal resolution of 20 seconds. The second group (group 2) includes a humidified nephelometer system (consisting of two nephelometers and a humidifier) that measures aerosol optical properties (scattering and back

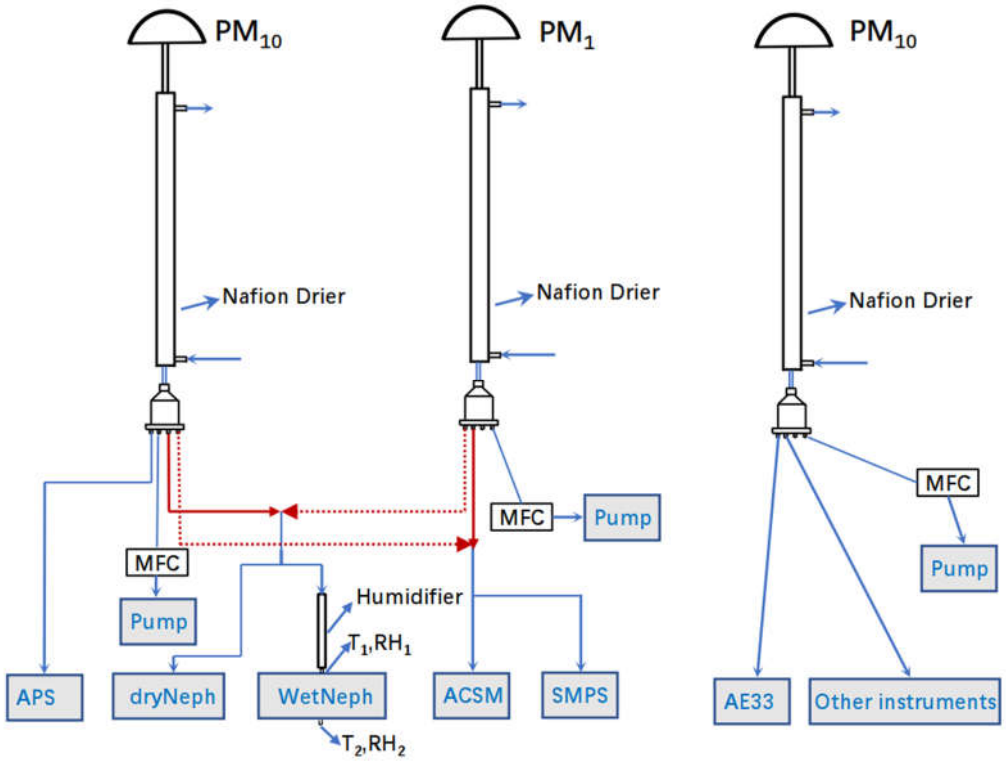

Figure 1. Schematic diagram of the inlet systems for aerosol sampling instruments

scattering coefficients at three wavelengths: 450 nm, 525 nm, 635 nm) of ambient aerosol particles in dry state (DryNeph) and under 85% RH condition (WetNeph). The third group (group3) includes two instruments, an ACSM and a scanning mobility particle sizer (SMPS; TSI model 3080). The CV-ToF-ACSM measures non-refractory particulate matter (NR-PM) species including organics, SO_4^{2-}, NO_3^-, NH_4^+, and Cl^- with an air flow of 0.1 L/min and a time resolution of 2 minutes. Since the CV-ToF-ACSM instrument comes with a $PM_{2.5}$ impactor, when the impactor of upstream is PM_{10}, chemical compositions of $PM_{2.5}$ rather than of PM_{10} were measured.

The SMPS measures particle mobility diameter size distributions with a diameter range of 12 nm to 760 nm. The inlets of group2 and group3 switch every 15 minutes, as denoted by the dashed and solid red lines in Fig.1, enabling the instruments of these two groups to alternately measure the

chemical and optical properties of PM_{10} and PM_1. The fourth group (group4) includes an AE33 aethalometer (Drinovec et al., 2015) and other aerosol instruments. Due to technical issues with the humidifier, the humified nephelometer system started to operate continuously since the 30th Nov.

2.2 The humidified nephelometer system

The humidified nephelometer system we built was set up to measure dry state aerosol optical properties at a fixed RH of 85%. The RH of the air sample is increased by a humidifier that consists of two layers. The inner layer is a Gore-Tex tube layer passing through sampled air, while the outer layer is a stainless-steel tube with circulating liquid water. The water vapor penetrates through the Gore-Tex tube and humidifies the sample air, while liquid water is kept from the inner layer by the Gore-Tex material. Upon the switch of inlets between group 2 and group 3, delays in valve switching caused instantaneous low pressure in the sample air, which broke the humidifier with the Gore-Tex tube after four days of continuous operation (3rd, Dec) and flooded the WetNeph. The WetNeph was fixed and recalibrated and a commercial Nafion drier (60 cm long, Perma Pure company) replaced the Gore-Tex tube, which works the same way but is more resistant to low pressure. The temperature of the circulating water layer is controlled by a water bath and specified by an algorithm that adjusts the water temperature to maintain a relatively constant RH in the sensing volume of the WetNeph. To monitor the RH in the sensing volume of the WetNeph, two temperature and RH sensors (Vaisala HMP110, with accuracies of ± 0.2 ℃ and ± 1.7 % for RH between 0 to 90%, respectively, and ± 2.5 % for RH between 90 to 100%) were placed at the inlet and outlet of the WetNeph. Defining measured RHs/temperatures at the inlet and outlet of the WetNeph as RH_1/T_1 and RH_2/T_2, the according dew point temperatures T_{d1} and T_{d2} can be calculated and the average value $\overline{T_d}$ was treated as the dew point of the sample air in the sensing volume of WetNeph. The sample RH is calculated using $\overline{T_d}$ and the sample temperature measured by a sensor inside the sample cavity of the nephelometer.

2.3 ACSM measurements and data analysis

The mass concentration and chemical composition of NR-PM species were measured with the Aerodyne ToF-ACSM which is equipped with a $PM_{2.5}$ aerodynamic lens (Williams et al., 2010) and a

capture vaporizer (CV) (Xu et al., 2017;Hu et al., 2017) to extend the measured particle size to 2.5 μm. Detailed instrument descriptions were given in Fröhlich et al. (2013) and Xu et al. (2017). The CV-ToF-ACSM data were analyzed with the standard data analysis software (Tofware v2.5.13, https://sites.google.com/site/ariacsm/) within Igor Pro (v6.37, WaveMetrics, Inc., Oregon, USA). The CV was designed with an enclosed cavity to increase particle collection efficiency (CE) at the detector (Xu et al., 2017). Both laboratory and field measurements indicate that the CE of CV was fairly robust and was roughly equivalent to 1. Therefore, a CE of 1 was applied to all measured species in this study (Hu et al., 2017; Hu et al., 2018b) (Hu et al., 2017;Hu et al., 2018b). Relative ionization efficiencies (RIEs) of 3.06 and 1.09 were used for ammonium and sulfate quantification respectively, and the default values of 1.1 and 1.4 were used for nitrate and organic aerosol (OA) respectively. Compared with the AMS with standard vaporizer, the CV-ToF-ACSM reports higher fragments at smaller *m/z*'s due to additional thermal decomposition associated with increased residence time and hot surface collisions (Hu et al., 2018a). As a result, f_{44} from CV-ToF-ACSM measurements is often much higher than those previously reported from AMS, yet they are well correlated (Hu et al., 2018a).

The organic mass spectra from *m/z* 12 to 214 were analyzed by positive matrix factorization (PMF) (Paatero and Tapper, 1994) with an Igor Pro based PMF evaluation tool (v3.04) (Ulbrich et al., 2009). The ion fragments *m/z* of 38, 49, 63 and 66 were removed from both PM_1 and $PM_{2.5}$ PMF inputs considering their small contributions to the total organic signals yet with high signal-to-noise ratios. The PMF results were then evaluated following the procedures detailed in Zhang et al. (2011). After carefully evaluating the mass spectral profiles, diurnal patterns and temporal variations of the OA factors and comparing them with other collocated measurements, a five-factor solution was selected for both PM_1 and $PM_{2.5}$. The five factors include four primary factors, i.e., hydrocarbon-like OA (HOA), cooking OA (COA), biomass burning OA (BBOA), and coal combustion OA (CCOA), and a secondary factor, oxygenated OA (OOA). More detailed descriptions on the PMF results will be given in He et al. (in preparation).

2.4 Data reprocessing

The size distributions measured by APS were converted to mobility-equivalent size distributions using spherical shape assumptions and an effective particle density of 1.7 g/cm^3. Note that the

designations of PM_{10} and PM_1 are in respect to aerosol aerodynamic diameters, while the corresponding mobility-equivalent cut diameters of the two impactors are approximately 7669 nm and 767 nm, respectively. For simplicity and consistency, we will continue to refer to them as the PM_{10} and PM_1 based on their aerodynamic diameter. For the case of PM_1 measurements, the mobility-equivalent cut diameter is quite near the upper range of the SMPS size range. Considering that the cut diameter of the impactor corresponds to the diameter of aerosol particles in ambient state (aerosol hygroscopic growth effect needs to be taken into account) and the SMPS measures the size distributions of aerosol particles in dry state, the SMPS measurements should be able to cover the full-size range of PM_1. When the SMPS was sampling aerosol particles of PM_{10}, the size distributions measured by SMPS and APS was merged together and truncated to an upper limit of 7669 nm to provide full range particle number size distributions (PNSD). In addition, the AE33 measures aerosol absorption coefficient at several wavelengths, the mass concentrations of black carbon (BC) were converted from measured aerosol absorption coefficients at 880 nm with a mass absorption coefficient of 7.77 m^2/g (Drinovec et al., 2015).

Since group 2 and 3 switched between PM_1 and PM_{10} inlets every 15 minutes, all measurements were averaged over each 15-minute observation episode, resulting in valid time resolutions of 15 minutes for APS and BC PM_{10} measurements and of 30 minutes for SMPS, CV-ToF-ACSM and the humidified nephelometer system PM_1 and PM_{10} measurements, respectively. This resulted in a 15-minute time lag between the averaged datasets of group 2 and group 3. To match the time of all the measurement data, the measurements of SMPS, ACSM and the humidified nephelometer system were linearly interpolated to the 15-minute time resolution of the APS data.

3 Methodology

3.1 Calculations of hygroscopicity parameters κ_{sca} and κ from measurements of the humidified nephelometer system

The humidified nephelometer system measures aerosol light scattering coefficients and backscattering coefficients at three wavelengths under dry state and 85% RH condition, providing measurements of the light scattering enhancement factor $f(\mathrm{RH},\lambda)$, which is defined as

$f(\mathrm{RH}=85\%,\lambda)=\frac{\sigma_{sp(RH,\ \lambda)}}{\sigma_{sp(dry\ \ \lambda)}}$, with λ being the light wavelength. In this study, we only calculate $f(\mathrm{RH},525\ \mathrm{nm})$ and refer to it hereinafter as $f(\mathrm{RH})$ for simplicity. Brock et al. (2016) proposed a single parameter formula to describe $f(\mathrm{RH},\lambda)$ as a function of RH. Kuang et al. (2017) further developed this parameterization scheme to better describe measured $f(\mathrm{RH})$ by including the reference RH (RH_0) in the dry nephelometer as shown in Eq.1, using which the optical hygroscopicity parameter κ_{sca} can be derived from $f(\mathrm{RH})_{measured}$.

$$f(\mathrm{RH})_{measured}=(1+\kappa_{sca}\frac{RH}{100-RH})/(1+\kappa_{sca}\frac{RH_0}{100-RH_0}) \quad (1)$$

An overall hygroscopicity parameter κ referred to as $\kappa_{f(\mathrm{RH})}$ can be retrieved from measured $f(\mathrm{RH})$ with the addition of simultaneously measured particle number size distribution (PNSD) and BC mass concentration (Chen et al., 2014;Kuang et al., 2017). The idea is to conduct an iterative calculation using the Mie theory and the κ-Köhler theory together to find a $\kappa_{f(\mathrm{RH})}$ that closes the gap between the simulated and the measured $f(\mathrm{RH})$. Details on the calculations of $\kappa_{f(\mathrm{RH})}$ can be found in Kuang et al. (2017).

3.2 Calculations of $\boldsymbol{\kappa_{chem}}$ from aerosol chemical composition measurements

For the calculation of aerosol hygroscopicity parameter κ based on measured chemical composition data ($\boldsymbol{\kappa_{chem}}$), detailed information on the chemical species are needed. The CV-ToF-ACSM can only provide bulk mass concentrations of SO_4^{2-}, NO_3^-, NH_4^+, Cl^- ions and organic components. For the inorganic ions, a simplified ion pairing scheme (as listed in Table 1) was used to convert ion mass concentrations to mass concentrations of corresponding inorganic salts (Gysel et al., 2007;Wu et al., 2016).

Table 1. Densities (ρ) and hygroscopicity parameters (κ) of inorganic salts used in this study

Species	NH_4NO_3	NH_4HSO_4	$(NH_4)_2SO_4$	NH_4Cl
ρ (g cm^{-3})	1.72	1.78	1.769	1.527
κ	0.58	0.56	0.48	0.93

Mass concentrations of SO_4^{2-}, NO_3^-, NH_4^+, Cl^- are thus specified into ammonium sulfate (AS), ammonium nitrate (AN), ammonium chloride (AC) and ammonium bisulfate (ABS), with the κ values of these salts specified according to (Wu et al., 2016) and Liu et al. (2014) (Table1). For a given

internal mixture of different aerosol chemical species, a simple mixing rule called Zdanovskii–Stokes–Robinson (ZSR) can be used for predicting the overall $\boldsymbol{\kappa_{chem}}$ on the basis of volume fractions of different chemical species (ε_i) (Petters and Kreidenweis, 2007):

$$\kappa_{chem} = \sum_i \kappa_i \cdot \varepsilon_i \qquad (2)$$

where κ_i and ε_i represent the hygroscopicity parameter κ and volume fraction of chemical component *i* in the mixture. Based on Eq.2, κ_{chem} can be calculated as follows:

$$\kappa_{chem} = \kappa_{AS}\varepsilon_{AS} + \kappa_{AN}\varepsilon_{AN} + \kappa_{ABS}\varepsilon_{ABS} + \kappa_{AC}\varepsilon_{AC} + \kappa_{BC}\varepsilon_{BC} + \kappa_{OA}\varepsilon_{OA} \qquad (3)$$

where κ_{OA} and ε_{OA} represent κ and volume fraction of total organics. Since black carbon is hydrophobic, κ_{BC} is assumed to be zero. With known $\boldsymbol{\kappa_{chem}}$, κ_{OA} can be calculated using the following formula:

$$\kappa_{OA} = \frac{\kappa_{chem} - (\kappa_{AS}\varepsilon_{AS} + \kappa_{AN}\varepsilon_{AN} + \kappa_{ABS}\varepsilon_{ABS} + \kappa_{AC}\varepsilon_{AC})}{\varepsilon_{OA}} \qquad (4)$$

The volume concentration of organics was calculated by assuming density of POA as 1 g/cm^3 and density of OOA as 1.4 g/cm^3 (Wu et al., 2016). For the calculation of the total volume concentration (V_{tot}), we have three approaches. The first approach is to sum up the volume concentrations of all chemical species (AS, AN, ABS, AC, BC and organics), where the volume concentration of BC was calculated by assuming a density of 1.7 g/cm^3 (Wu et al., 2016). We refer the calculated total volume concentration of aerosol particles to as $V_{tot,Chem}$. The second approach is to integrate V_{tot} from measured PNSD using the equation $V_{tot,PNSD} = \int \frac{4}{3}\pi r^3 n(r) dr$, where r is the particle radius and n(r) is the measured particle number concentrations. The third approach is to use the trained machine learning estimator to estimate the V_{tot} based on measurements of dry nephelometer ($V_{tot,Neph}$) as was introduced in Kuang et al. (2018). V_{tot} of PM_1 calculated using these three methods were compared to each other and shown in Fig.S2. $V_{tot,Chem}$ correlates well with $V_{tot,PNSD}$, but it is on average 30% lower than that of $V_{tot,PNSD}$. Chemical components within aerosol particles such as dust, sea salt as well as metal ions cannot be detected by CV-ToF-ACSM. Since the Gucheng site is far from the ocean, sea salt should have negligible impacts on the total mass of PM_1. However, mineral dust can extend into the submicron range (Shao et al., 2007), which might be the cause for the low $V_{tot,Chem}$. calculated using CV-ToF-ACSM and BC data. $V_{tot,Neph}$ also correlates well with $V_{tot,PNSD}$, but is on

average 16% lower than that of $V_{tot,PNSD}$. Closure studies between modelled and measured σ_{sp} and σ_{bsp} at 525 nm for PM_1 and PM_{10} aerosol particles all showed good agreement between theoretical modelling results and measurements (Fig.S1), with most points falling within the 20% relative deviation lines. However, modelled σ_{sp} for both PM_1 and PM_{10} were obviously higher than measured σ_{sp}, with an average relative difference of 22% and 13% between them for PM_{10} and PM_1, respectively. The result for PM_1 explains why $V_{tot,Neph}$ was lower than $V_{tot,PNSD}$. Two reasons might have contributed to this discrepancy: (1) both PNSD and aerosol optical property measurements carry non-negligible uncertainties, with the SMPS bearing measurement uncertainty of 30% for particles larger than 200 nm, which contribute most to V_{tot} (Wiedensohler et al., 2012), and the nephelometer measured σ_{sp} having an uncertainty of 9% (Sherman et al., 2015;Titos et al., 2016); (2) The sampling tube length, valves, tube angles and flow rates are different for the dry nephelometer and SMPS (e.g. much shorter tube and smaller flow rate for SMPS than those for the dry nephelometer), leading to different wall loss and loss in semi-volatile aerosol components. ACSM and the dry nephelometer had a similar tube length and nephelometer measurements bear less uncertainty than SMPS. Thus, $V_{tot,Neph}$ was chosen as V_{tot} in the calculations of Eq.4. Based on the calculated V_{tot}, the material unidentified by CV-ToF-ACSM accounts for 19% of V_{tot} on average, could not be neglected in the κ_{OA} calculation. Thus, Eq.4 was modified as follows:

$$\kappa_{Org} = \frac{\kappa_{chem} - (\kappa_{AS} \cdot \varepsilon_{AS} + \kappa_{AN} \cdot \varepsilon_{AN} + \kappa_{ABS} \cdot \varepsilon_{ABS} + \kappa_X \cdot \varepsilon_X)}{\varepsilon_{Org}} \qquad (5)$$

where κ_X and ε_X are hygroscopicity parameter κ and volume fraction of the unidentified material. Previous studies using $V_{tot,Chem}$ as the total volume concentration of aerosol particles have avoided the discussion about influences of unidentified material by the CV-ToF-ACSM or other aerosol mass spectrometer instruments. The hygroscopicity of these unidentified materials, which might be dust or other components in continental regions, was not discussed before. Dust is nearly hydrophobic, with mineral dust showing κ in range of 0.01 to 0.08 (Koehler et al., 2009). In this paper, we arbitrarily specified κ_X to be 0.05.

3.3 Can $\kappa_{f(\mathrm{RH})}$ represent κ_{chem}?

According to Eq.5, the measured bulk κ_{chem} values are needed to derive κ_{OA}. Bulk aerosol chemical compositions and aerosol hygroscopicity $\kappa_{f(\mathrm{RH})}$ measurements are available, one might

naturally jump to the conclusion of treating $\kappa_{f(\mathrm{RH})}$ as κ_{chem} to derive κ_{OA} because both $\kappa_{f(\mathrm{RH})}$ and κ_{chem} are from bulk aerosol measurements. However, the relationship between κ_{chem}, $\kappa_{f(\mathrm{RH})}$ and the size-resolved κ distribution needs to be clarified in order to answer the question whether $\kappa_{f(\mathrm{RH})}$ can accurately represent κ_{chem}. The physical meanings of used different κ representations in the following discussions are listed in Table 2.

Table 2. Different κ and their physical meanings

$\kappa_{f(\mathrm{RH})}$	A uniform κ for all particle sizes which describes $f(\mathrm{RH})$ accurately
κ_{chem}	A bulk κ assuming different chemical compositions of aerosol populations are internally mixed and calculated with the ZSR mixing rule
κ_i	hygroscopicity parameter κ of chemical species *i*
κ_{D_p}	The κ assuming different chemical compositions of particles with diameter of D_p are internally mixed and calculated with the ZSR mixing rule

Using V_i to represent volume concentrations of chemical species *i* and $V_i(D_p)$ to represent volume concentrations of species *i* with diameter of D_p, κ_{chem} can be derived as follows based on Eq.2,:

$$\kappa_{chem} = \sum_i \kappa_i \cdot \varepsilon_i = \sum_i \frac{V_i}{V_{tot}} \cdot \kappa_i = \sum_i \frac{1}{V_{tot}} \cdot \int \frac{d\,V_i\,(D_p)}{dlogD_p} \cdot dlogD_p \cdot \kappa_i. \quad (6)$$

By swapping the order of summation and integration, Eq.6 can be written as:

$$\kappa_{chem} = \int \frac{1}{V_{tot}} \cdot \sum_i \frac{d\,V_i\,(D_p)}{dlogD_p} \cdot dlogD_p \cdot \kappa_i. \quad (7)$$

Considering that $\kappa_{D_p} = \sum_i \frac{dV_i\,(D_p)}{dV(D_p)} \cdot \kappa_i$, Eq.7 can be rewritten as:

$$\kappa_{chem} = \frac{1}{V_{tot}} \int \kappa_{D_p} \cdot dV(D_p) \quad (8)$$

Result of Eq.8 indicates that κ_{chem} calculated using Eq.3 represents the overall hygroscopicity of aerosol particles with volume contribution as the weighting function of κ_{D_p}.

As for $\kappa_{f(\mathrm{RH})}$, a detailed analysis is performed here to facilitate its physical understanding. The differential form of σ_{sp} of aerosol particles in dry state can be expressed as follows:

$$\sigma_{sp} = \int \frac{d\sigma_{sp}}{dlogD_p} dlogD_p \quad (9)$$

Based on the definition of $f(\mathrm{RH})$, σ_{sp} of aerosol particles under different RH conditions can be

written as:

$$\sigma_{sp}(RH) = \int \frac{d\sigma_{sp}}{dlogD_p} \cdot f_{D_p}(RH) \cdot dlogD_p \quad (10)$$

Therefore, the differential form of observed overall $f(\mathrm{RH})$ can be formulated as:

$$f(\mathrm{RH}) = \int \frac{1}{\sigma_{sp}} \cdot \frac{d\sigma_{sp}}{dlogD_p} \cdot f_{D_p}(RH) \cdot dlogD_p \quad (11)$$

Based on this formula, the sensitivity of $f(\mathrm{RH})$ on the hygroscopicity of aerosol particles with diameter D_p (κ_{D_p}) can be derived as:

$$\frac{1}{dlogD_p} \cdot \frac{\partial f(\mathrm{RH})}{\partial \kappa_{D_p}} = \frac{1}{\sigma_{sp}} \cdot \frac{d\sigma_{sp}}{dlogD_p} \cdot \frac{\partial f_{D_p}(RH)}{\partial \kappa_{D_p}} \quad . \quad (12)$$

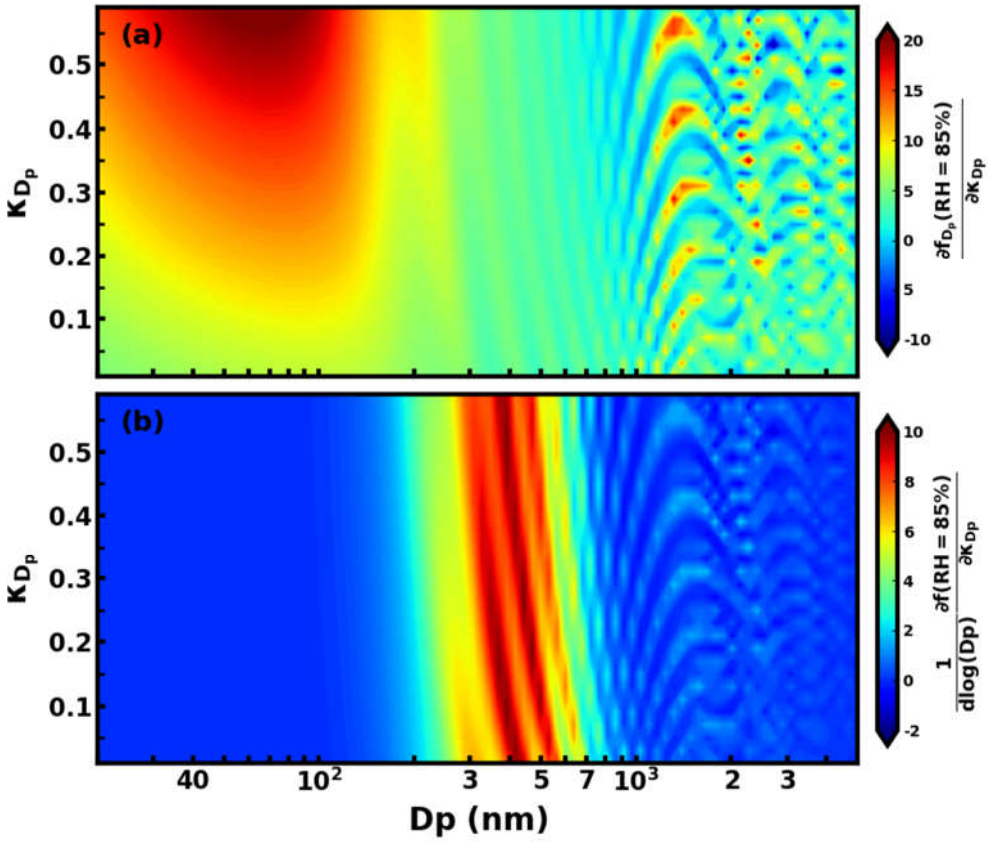

Figure 2. (a) simulated $\frac{\partial f_{D_p}(RH)}{\partial \kappa_{D_p}}$; (b) simulated $\frac{1}{dlogD_p} \cdot \frac{\partial f(\mathrm{RH})}{\partial \kappa_{D_p}}$

The sensitivity of $f(\mathrm{RH})$ to κ_{D_p} are determined together by the two terms in Eq. 12: (1) $\frac{1}{\sigma_{sp}} \cdot \frac{d\sigma_{sp}}{dlogD_p}$, which represents the contribution of σ_{sp} of aerosol particles in dry state with diameter D_p to total

σ_{sp}, and (2) $\frac{\partial f_{D_p}(RH)}{\partial \kappa_{D_p}}$, which represents the sensitivity of $f_{D_p}(RH)$ to κ_{D_p}. Based on the Mie theory and the κ-Köhler theory, we simulated the second term under 85% RH condition for varying D_p and κ_{D_p} values (Fig.2a). In the diameter range below 200 nm, $\frac{\partial f_{D_p}(RH)}{\partial \kappa_{D_p}}$ is very high, displaying a maximum near 60 nm. In this diameter range, larger κ_{D_p} generally corresponds to higher $\frac{\partial f_{D_p}(RH)}{\partial \kappa_{D_p}}$. For $200\ \text{nm} < D_p < 800\ \text{nm}$, higher and lower $\frac{\partial f_{D_p}(RH)}{\partial \kappa_{D_p}}$ appear alternatively, with all values staying positive. For $D_p > 800\ nm$, maxima and minima regions appear alternatively, and $f_{D_p}(RH)$ might decrease with increasing κ_{D_p}. This is because, at this diameter range, the aerosol scattering efficiency has a non-monotonic response to the particle diameter increase (see Fig.2a of (Kuang et al., 2018)).

The first term of Eq.9, representing size-resolved σ_{sp} contributions of particles with diameter in dry state, mainly depends on the PNSD. The average PNSD of PM_{10} was applied in the simulation of the first term using Mie theory (Fig.S3). Combining results of the first term and second term, the sensitivity of $f(\text{RH})$ to κ_{D_p} was obtained and depicted in Fig.2b. Results reveal that $f(\text{RH})$ is quite sensitive to the κ_{D_p} of particles within 200 to 800 nm diameter range, but almost insensitive to κ_{D_p} of particles with diameters below 200 nm and above 800 nm (corresponding aerodynamic diameter of about 1 μm). For particles smaller than 200 nm, the first term was quite small especially for particles smaller than 100 nm (Fig.S3), while for particles larger than 800 nm, in addition to a small first term, the second term fluctuated between negative and positive values, which is why $f(\text{RH})$ was not sensitive to the overall hygroscopicity of these larger aerosol particles. These results suggest that although $\kappa_{f(\text{RH})}$ was derived from $f(\text{RH})$ measurements of PM_{10}, it mainly represents the overall hygroscopicity of aerosol particles with dry diameters between 200 and 800 nm for continental aerosols. This result indicates that $\kappa_{f(\text{RH})}$ derived from $f(\text{RH})$ measurements of PM_{10} and PM_1 should differ little from each other for measurements conducted in continental regions.

However, the quantitative relationship between $\kappa_{f(\text{RH})}$ and size-resolved κ_{D_p} is still not clear. Based on Eq.11, $f_{D_p}(RH)$ can be expressed as:

$$f_{D_p}(RH) = \frac{d\sigma_{sp}(RH)}{d\sigma_{sp}} = \frac{\frac{1}{4}\cdot\pi\cdot(D_p\cdot g)^2\cdot Q_{sca}(D_p,g)\cdot dN}{d\sigma_{sp}}, \quad (13)$$

where g is the growth factor of aerosol particles which is a function of κ_{D_p} and RH (Brock et al., 2016), i.e. $g = (1 + \kappa_{D_p} \cdot \frac{RH}{100-RH})^{1/3}$, dN is differential form of aerosol number concentration, and Q_{sca} is the scattering efficiency as a function of D_p and g. The results of Kuang et al. (2018) indicate that, under dry state, Q_{sca} can be expressed as $Q_{sca} = k \cdot D_p$ with k varying as a function of D_p. Here, we follow this idea and express the Q_{sca} under humidified condition as $Q_{sca}(D_p, g) = \mathrm{C} \cdot D_p \cdot g$, where C is a function of D_p, κ_{D_p} and RH. Replacing g and Q_{sca} in Eq.13, we yield:

$$f_{D_p}(RH) = \frac{\frac{1}{4}\cdot\pi\cdot {D_p}^3\cdot C(\mathrm{Dp},\kappa_{D_p},\mathrm{RH})\cdot(1+\kappa_{D_p}\cdot\frac{RH}{100-RH})\cdot dN}{d\sigma_{sp}}, \quad (14)$$

which we can substitute into Eq.8, to obtain a new expression for $f(\mathrm{RH})$:

$$f(\mathrm{RH}) = \int \frac{\frac{1}{4}\cdot\pi\cdot {D_p}^3\cdot C(\mathrm{Dp},\kappa_{D_p},\mathrm{RH})\cdot(1+\kappa_{D_p}\cdot\frac{RH}{100-RH})\cdot dN}{\sigma_{sp}} \quad (15)$$

If we define $X_c(\mathrm{Dp},\kappa_{D_p},\mathrm{RH}) = C(\mathrm{Dp},\kappa_{D_p},\mathrm{RH})/\mathrm{k}$, and considering that $d\sigma_{sp} = \frac{1}{4}\cdot\pi\cdot {D_p}^2\cdot Q_{sca}\cdot dN = \frac{1}{4}\cdot\pi\cdot {D_p}^3\cdot \mathrm{k}\cdot dN$, Eq.14 can be written as:

$$f(\mathrm{RH}) = \int \frac{X_c(\mathrm{Dp},\kappa_{D_p},\mathrm{RH})\cdot(1+\kappa_{D_p}\cdot\frac{RH}{100-RH})\cdot d\sigma_{sp}}{\sigma_{sp}} \quad (16)$$

The $\kappa_{f(\mathrm{RH})}$ is a uniform κ for aerosol particle sizes that can yield simulated $f(\mathrm{RH})$ equal to the measured one. Thus, $f(\mathrm{RH})$ can also be expressed as:

$$f(\mathrm{RH}) = \int \frac{X_c(\mathrm{Dp},\kappa_{f(\mathrm{RH})},\mathrm{RH})\cdot(1+\kappa_{f(\mathrm{RH})}\cdot\frac{RH}{100-RH})\cdot d\sigma_{sp}}{\sigma_{sp}} \quad (17)$$

Combining Eq.16 and Eq.17, the relationship between $\kappa_{f(\mathrm{RH})}$ and size-resolved κ_{D_p} can be derived as:

$$\kappa_{f(\mathrm{RH})} = \frac{\int X_c(\mathrm{Dp},\kappa_{D_p},\mathrm{RH})\cdot\kappa_{D_p}\cdot d\sigma_{sp}}{\int X_c(\mathrm{Dp},\kappa_{f(\mathrm{RH})},\mathrm{RH})\cdot d\sigma_{sp}} + \frac{\int (X_c(\mathrm{Dp},\kappa_{D_p},RH) - X_c(\mathrm{Dp},\kappa_{f(\mathrm{RH})},\mathrm{RH}))\cdot d\sigma_{sp}}{\int X_c(\mathrm{Dp},\kappa_{f(\mathrm{RH})},\mathrm{RH})\cdot d\sigma_{sp}} \cdot \frac{100-RH}{RH}. \quad (18)$$

X_c values under 85% RH for different D_p and κ_{D_p} values are simulated and shown in Fig.3, based

on this result of X_c the second term of Eq.18 (which depends on the PNSD and size-resolved κ_{D_p})

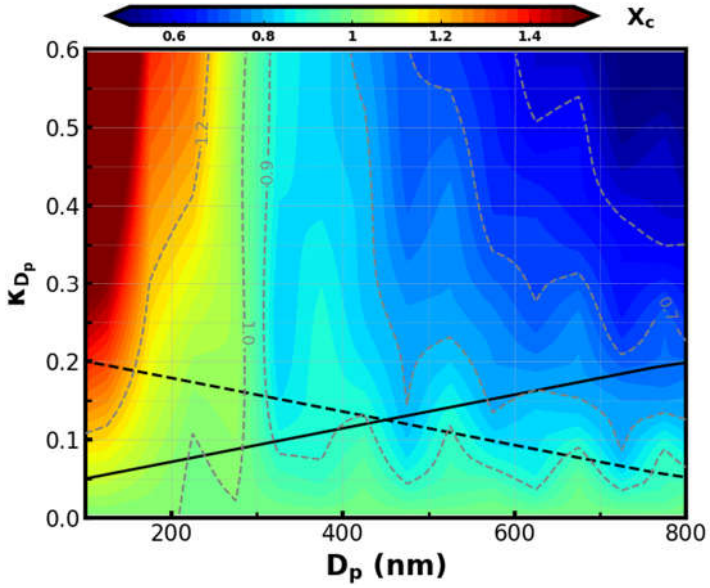

Figure 3. Simulated values of X_c under 85% RH for different D_p and κ_{D_p} values. Black solid and dashed lines are two assumed size-resolved κ_{D_p} distributions.

could be calculated using the average PNSD during this field campaign and two assumed extreme cases of size-resolved κ_{D_p} (solid and dashed black lines in Fig.3). For PM_1, the second term corresponding to the two size-resolved κ_{D_p} cases were -0.007 and 0.008, respectively. Corresponding values simulated for PM_{10} were -0.005 and 0.004, respectively. To further investigate the possible contribution range of the second term to $\kappa_{f(\mathrm{RH})}$, size-resolved κ_{D_p} derived by Liu et al. (2014) based on size resolved chemical composition measurements in ambient atmosphere on the NCP region (Fig.S4) were used with the average PNSD during this campaign to calculate values of the second term. Calculated values of second term ranged from -0.005 to 0.009, with its contribution to $\kappa_{f(\mathrm{RH})}$ ranging from -1.5% to 2% (0.3% on average). These results indicate that the second term was negligible in most cases, and Eq.18 could be approximated as:

$$\kappa_{f(\mathrm{RH})} \approx \frac{\int X_c(\mathrm{Dp},\kappa_{D_p},\mathrm{RH})\cdot\kappa_{D_p}\cdot d\sigma_{sp}}{\int X_c(\mathrm{Dp},\kappa_{f(\mathrm{RH})},\mathrm{RH})\cdot d\sigma_{sp}} \quad (19)$$

X_c values shown in Fig.3 indicate that for aerosol particles in the diameter range of 200 to 800 nm (which contribute most to σ_{sp} and are the part of the aerosol population that $\kappa_{f(\mathrm{RH})}$ is most sensitive to) and for the observed κ_{D_p} range of continental aerosols (κ_{D_p}usually less than 0.5), X_c mainly ranged from 0.7 to 1. Considering this, we might approximately assume X_c in Eq.18 as a constant value. Then, Eq.19 can be further simplified to:

$$\kappa_{f(\mathrm{RH})} \approx \frac{1}{\sigma_{sp}} \int \kappa_{D_p} \cdot d\sigma_{sp} \qquad (20)$$

This result suggests that $\kappa_{f(\mathrm{RH})}$ can be approximately understood as the overall hygroscopicity of aerosol particles with the σ_{sp} contribution as the weighting function of κ_{D_p}.

Based on results of Eqs.8 and 20, both $\kappa_{f(\mathrm{RH})}$ and κ_{chem} represent the overall hygroscopicity of bulk aerosol particles, however, their weighting functions of κ_{D_p} are different. Within a certain D_p range, aerosol σ_{sp} is approximately proportional to aerosol volume (Kuang et al., 2018), resulting in little difference between $\kappa_{f(\mathrm{RH})}$ and κ_{chem}. In this study, bulk $\kappa_{f(\mathrm{RH})}$ was measured for both PM_1 and PM_{10}. How much does κ_{chem} differ from $\kappa_{f(\mathrm{RH})}$ for PM_1 and PM_{10} samples? Both PNSD and size-resolved κ_{D_p} distributions contribute to the difference between κ_{chem} and $\kappa_{f(\mathrm{RH})}$. To study

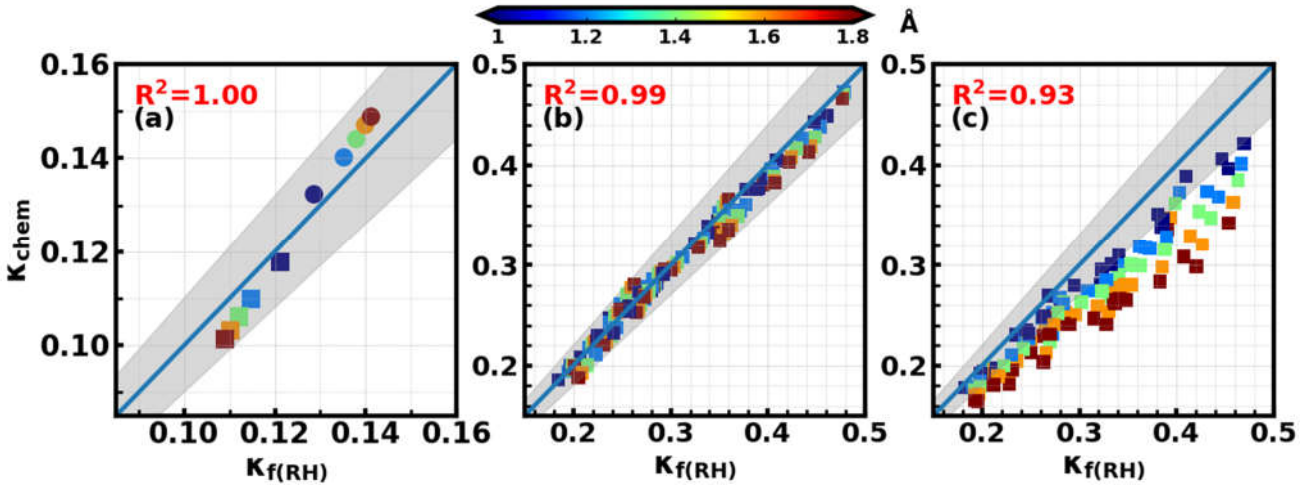

Figure 4. κ_{chem} versus $\kappa_{f(\mathrm{RH})}$, colors represent average Ångström exponent (Å) values of corresponding PNSD (a)corresponding to size-resolved κ_{D_p} distributions shown in Fig.3 (squares correspond to the solid line in Fig.3 and circles correspond to the dashed line in Fig.3); (b) and (c) corresponding to size-resolved κ_{D_p} distributions shown in Fig.S4 for PM1 and PM10, respectively. Gray areas represent the absolute relative differences between κ_{chem} and $\kappa_{f(\mathrm{RH})}$ less than 10%.

their influences in a simple and apparent way, κ_{chem} and $\kappa_{f(\mathrm{RH})}$ were simulated based on the two extreme cases of size-resolved κ_{D_p} distributions in Fig. 3 and five average PNSDs corresponding to five ranges of aerosol Ångström exponent (0.9-1.1,1.1-1.3,1.3-1.5,1.5-1.7,1.7-1.9) during this field campaign. In the instance of PM_1, as can be seen in Fig.4a, assuming a κ_{D_p} increasing as a function of D_p resulted in $\kappa_{chem}<\kappa_{fRH}$ (square points in Fig.4a), especially for PNSDs corresponding to larger Ångström exponents. This is because the volume contributions of small particles (e.g. particles with D_p between 100 to 300 nm) to V_{tot} are larger than their light scattering coefficient contributions

417 to σ_{sp} (as shown in Fig.S6), thus the hygroscopicity of small particles had larger impacts on κ_{chem}
418 than κ_{fRH}. Higher Ångström exponents generally correspond to shift in PNSD towards smaller D_p,
419 which exacerbates the contribution of small particles, further increasing the difference between κ_{chem}
420 and κ_{fRH}. For the case with κ_{D_p} decreasing as a function of D_p (circle markers in Fig.4a) it is vice
421 versa, resulting in $\kappa_{chem} > \kappa_{fRH}$. In general, for these two extreme cases of size-resolved κ_{D_p}
422 distributions, the absolute value of the relative difference between κ_{chem} and $\kappa_{f(\mathrm{RH})}$ ranged from
423 2.8% to 7.5% with an average of 4.8%. This result indicates that for PM_1, κ_{chem} might differ little
424 from $\kappa_{f(\mathrm{RH})}$ since κ_{D_p} usually varies less with D_p in ambient atmosphere than in the two assumed
425 cases (Liu et al., 2014). The average size-resolved κ_{D_p} distribution from Haze in China campaign
426 (Liu et al., 2014) indicate that κ_{D_p} varies significantly for D_p<250 nm, while it varies less within the
427 diameter range of 250 nm to 1 μm. To further study the variation range of the relative difference
428 between κ_{chem} and $\kappa_{f(\mathrm{RH})}$ under ambient conditions, the size-resolved κ_{D_p} distributions derived
429 from measured size-resolved chemical compositions in the NCP region (Liu et al., 2014) (shown in
430 Fig.S5) were used in simulations and results are shown in Fig.4b. The absolute value of the relative
431 difference between κ_{chem} and $\kappa_{f(\mathrm{RH})}$ ranged from 0.04% to 8% with an average and standard
432 deviation of $2.8\pm2\%$, which further confirms that for PM_1 $\kappa_{f(\mathrm{RH})}$ can accurately represent κ_{chem} in
433 most cases.

434 For PM_{10}, values of κ_{chem} and $\kappa_{f(\mathrm{RH})}$ using κ_{D_p} size distributions derived from ambient
435 measurements (Fig.S5, similar to Fig.4b) were simulated and displayed in Fig.4c. The simulated
436 absolute values of the relative difference between κ_{chem} and $\kappa_{f(\mathrm{RH})}$ ranged from 0.2% to 41% with
437 an average and standard deviation of 16 ± 8 %, with all κ_{chem} lower than $\kappa_{f(\mathrm{RH})}$. This is because, for
438 PM_{10}, super-micron particles typically with low hygroscopicity (Fig.S5) contribute much more to V_{tot}
439 than to σ_{sp} (as shown in Fig.S7). These results indicate that, for PM_{10}, $\kappa_{f(\mathrm{RH})}$ cannot accurately
440 represent κ_{chem}.

441 Above analysis results indicate that $\kappa_{f(\mathrm{RH})}$ retrieved from light scattering measurements of PM_1
442 represent accurately the κ_{chem} of PM_1 and can be used in Eq.5 as measured κ_{chem} for deriving κ_{OA}.

4 Results and discussions

4.1 Overview of the campaign data

The time series of ambient RH, chemical compositions of $PM_{2.5}$ and PM_1, σ_{sp} at 525 nm of PM_{10} and PM_1 in dry state, calculated κ_{sca} and $\kappa_{f(\mathrm{RH})}$ values of PM_{10} and PM_1 are shown in Fig.5. Overall, the mass concentrations of NR-PM_1 and NR-$PM_{2.5}$ ranged from 1 to 221 $\mu g/m^3$ and from 1.8 to 326 $\mu g/m^3$, with average concentrations of 63 and 93 $\mu g/m^3$, respectively. Measured σ_{sp} at 525 nm of PM_1 and PM_{10} ranged from 11 to 1875 Mm^{-1} and from 18 to 2732 Mm^{-1}, with average values of 550 and 814 Mm^{-1}, respectively. These results demonstrate that this campaign was carried out at a site that is overall highly polluted, where quite clean conditions as well as extremely polluted conditions were experienced during the measurement period. The mass contributions of ammonium, nitrate, sulfate and organics to NR-$PM_{2.5}$ and NR-PM_1 are listed in Table 3 with organics being the major fraction of NR-PM_1 and NR-$PM_{2.5}$.

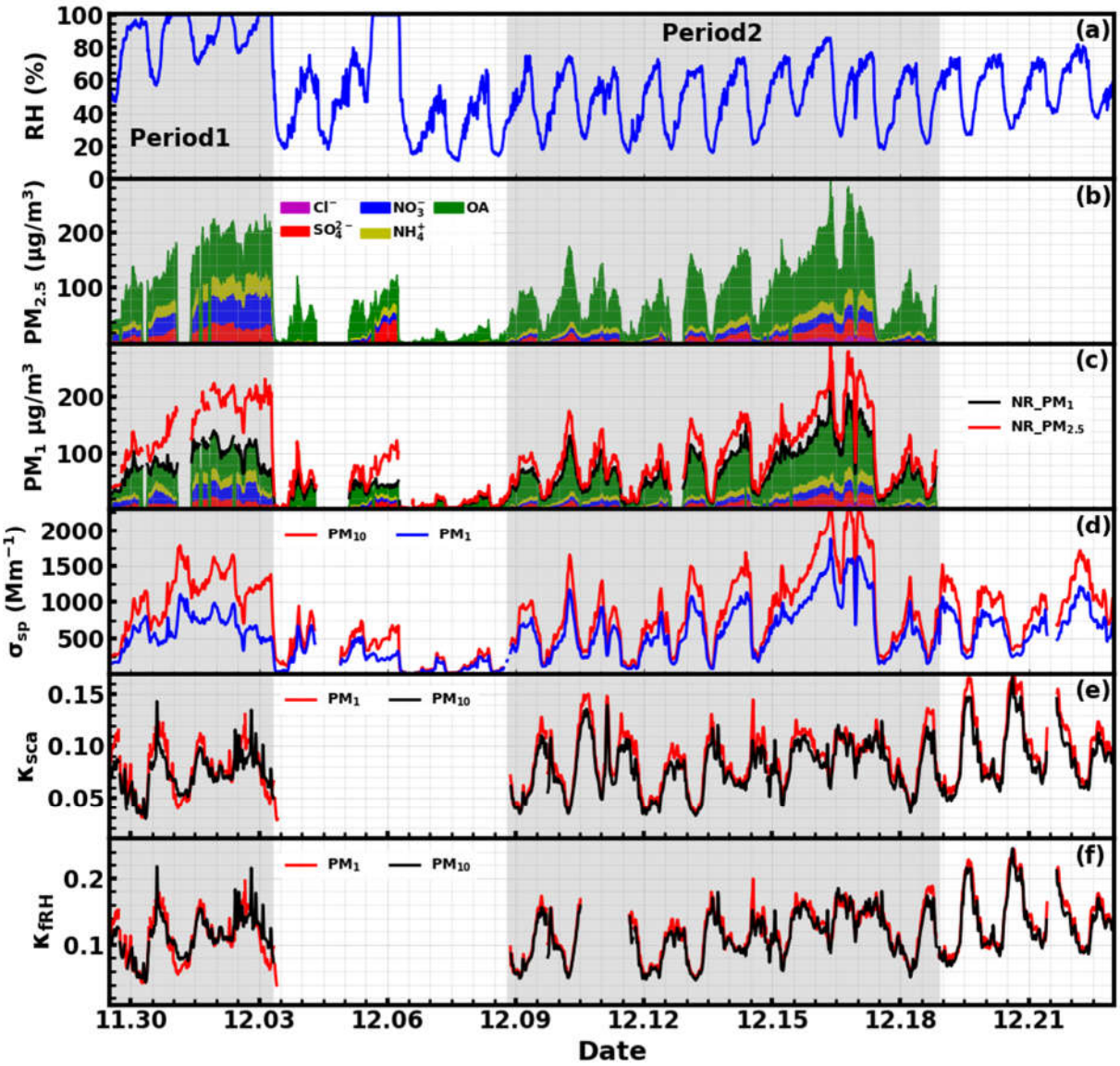

Figure 5. Time series of ambient RH (a), chemical compositions of $PM_{2.5}$ (b) and PM_1 (c), σ_{sp} at 525 nm of PM_{10} and PM_1 (d), calculated κ_{sca} (e) and $\kappa_{f(\mathrm{RH})}$ (f) values of PM_{10} and PM_1.

During period 1 shown in Fig.5, nitrate contributed most to inorganics, while inorganics contribute most to mass concentrations of NR-$PM_{2.5}$ and NR-PM_1. During the period 2 shown in Fig.5, the ambient RH is relatively lower than that of the first period, ranging from 16% to 86% with an average of 49%. During this period, organics contributed most to mass concentrations of NR-$PM_{2.5}$ and NR-PM_1, with the NR mass concentrations of $PM_{2.5}$ and σ_{sp} at 525 nm of PM_{10} being only 33% and 40% higher than those of PM_1.

The time series of calculated κ_{sca} and $\kappa_{f(\mathrm{RH})}$ are shown in Fig.5e-f. κ_{sca} of PM_1 and PM_{10} ranged from 0.01 to 0.2, and from 0.02 to 0.17, with corresponding averages of 0.09 and 0.08, respectively. The $\kappa_{f(\mathrm{RH})}$ was not available from 12:00 10th Dec to 12:00 11th Dec due to the absence

of PNSD measurements. $\kappa_{f(\mathrm{RH})}$ of PM_1 and PM_{10} ranged from 0.02 to 0.27, and from 0.03 to 0.26, with corresponding averages of 0.12 and 0.12, respectively. These results indicate that the hygroscopicity during this campaign was generally low, which could be associated with the high mass contributions of organics. The range as well as the average level of $\kappa_{f(\mathrm{RH})}$ is quite consistent with the results obtained at the same site in winter 2016, suggesting the prevalent low aerosol hygroscopicity conditions in winter at this site. Additionally, it can be noted that except for fog events, κ_{sca} and $\kappa_{f(\mathrm{RH})}$ values of PM_1 are generally higher than those of PM_{10}, yet the differences are small (10% and 3.5% for κ_{sca} and $\kappa_{f(\mathrm{RH})}$, respectively). Although particles with diameters above 800 nm impact almost negligibly on retrieved $\kappa_{f(\mathrm{RH})}$ (refer to discussions in Sect3.3), it can still cause a small difference between $\kappa_{f(\mathrm{RH})}$ of PM_{10} and PM_1. Results of previous studies indicate that the overall hygroscopicity of aerosol particles larger than 800 nm are usually low and are typically lower than the overall hygroscopicity of accumulation mode particles (Liu et al., 2014), which may explain why $\kappa_{f(\mathrm{RH})}$values of PM_1 are generally higher than those of PM_{10} during non-fog periods (periods with RH <100%).

Table 3. Average (range) mass contribution of ammonium, nitrate, sulfate and organics to NR-$PM_{2.5}$ and NR-PM_1 during different periods.

Species	Ammonium		nitrate		sulfate		Organics	
	PM_1	$PM_{2.5}$	PM_1	$PM_{2.5}$	PM_1	$PM_{2.5}$	PM_1	$PM_{2.5}$
Entire period	12% 0.2-24%	12% 0.1-24%	13% 2-31%	14% 1-32%	10% 0.3-49%	11% 0.2-50%%	59% 12-99%	59% 4-91%
Period 1 Fog	15% 10-17%	16% 12-18%	22% 11-28%	24% 16-30%	13% 9-15%	14% 12-16%	47% 30-65%	42% 37-55%
Period 1 non-fog	17% 10-22%	16% 7-21%	23% 6-31%	23% 5-32%	12% 8-23%	12% 7-17%	43% 32-75%	44% 31-69%
Period 2	12% 0.2-20%	10% 0.1-19%	11% 5-30%	10% 4-29%	8% 0.3-16%	7% 0.2-16%	64% 40-82%	67% 40-85%

During fog periods, a large part of submicron particles in dry state will be activated into fog droplets, which are super micron particles in ambient state (see PNSD examples in Fig.S4a), exerting substantial impacts on $f(\mathrm{RH})$ measurements of PM_{10} which are not detectable in the PM_1

measurements. Since for a certain particle diameter and fog supersaturation, particles with higher hygroscopicity are more readily activated, the observed PM_{10} $\kappa_{f(RH)}$ increased during fog events and often exceeded those of PM_1 in contrast to non-fog periods (Fig.5f).

4.2 κ_{OA} derivations and its relationship with organic aerosol oxidation state

The results in Sect.3.3 demonstrate that $\kappa_{f(RH)}$ of PM_1 accurately represents κ_{chem} in most cases, thus a closure study between calculated κ_{chem} of PM_1 based on measured chemical compositions and measured κ_{chem} (represented by PM_1 $\kappa_{f(RH)}$) can be conducted using Eq.3 if κ_{OA} was known. A κ_{OA} of 0.06 was used in this closure test, which was calculated by Wu et al. (2016) based on aerosol chemical composition and aerosol hygroscopicity measurements. As shown in Fig.6a, the comparison between measured and calculated κ_{chem} has not achieved very good agreements. We

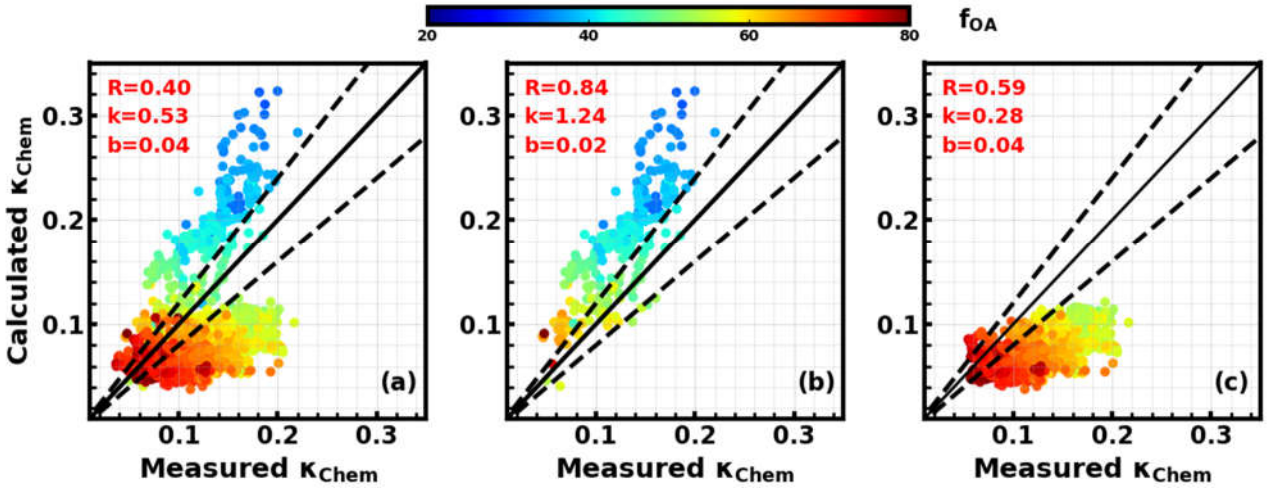

Figure 6. Comparison between measured and calculated κ_{chem} by assuming a κ_{Org} of 0.06. **(a)** The whole period; **(b)** Only Period 1; **(c)** Only Period 2. Colors represents the mass fractions of organic aerosol in NR-PM_1 (f_{OA}), and the color bar is shown on the top.

notice that the calculated κ_{chem} was overestimated when mass fraction of organic aerosol (f_{OA}) was lower than 45%, while it was underestimated when f_{OA} was higher than 45%. As described in Sect.4.1, these two situations roughly correspond to Period 1 and 2, respectively. Separating the data points shown in Fig.6a into Periods 1 (Fig.7b) and 2 (Fig.7c), it can be seen that all low f_{OA} data points are found in Period 1, with most of the data points showing f_{OA} less than 50%. Although the calculated κ_{chem} during this period was on average 25% higher than the measured κ_{chem}, they were highly correlated (R=0.84). A similar case was also found in Wu et al. (2013), and they concluded that the loss of semi-volatile ammonium nitrate in the HTDMA might be the reason. The relationship

between nitrate concentration and the difference between calculated and measured κ_{chem} was investigated, which confirmed the influence of nitrate on this discrepancy (Fig.S7), and the overestimation of calculated κ_{chem} due to the volatile loss of ammonium nitrate. Since the tube length (from the splitter to inlet of instrument) of wet nephelometer was about 1 m longer than that of the CV-ToF-ACSM, there probably was more loss in ammonium nitrate in the wet nephelometer.

During Period 2, the average mass fraction of nitrate was low (11%), and the loss of ammonium nitrate had minor influence on κ_{chem} estimations (Fig.S7). However, when organic aerosol was dominant during Period 2, the calculated κ_{chem} was underestimated in most cases (Fig.6c). Previous studies have shown larger κ_{OA} for OA with higher oxidation level (Chang et al., 2010;Duplissy et al., 2011;Wu et al., 2013), which might have contributed to the underestimation in κ_{chem}. This gave us the hint that Period 2 might provide us a good opportunity to study κ_{OA}. Following the method in Sect. 3.2, κ_{OA} was derived using Eq.5, resulting in a κ_{OA} ranging from 0.0 to 0.25, with an average of

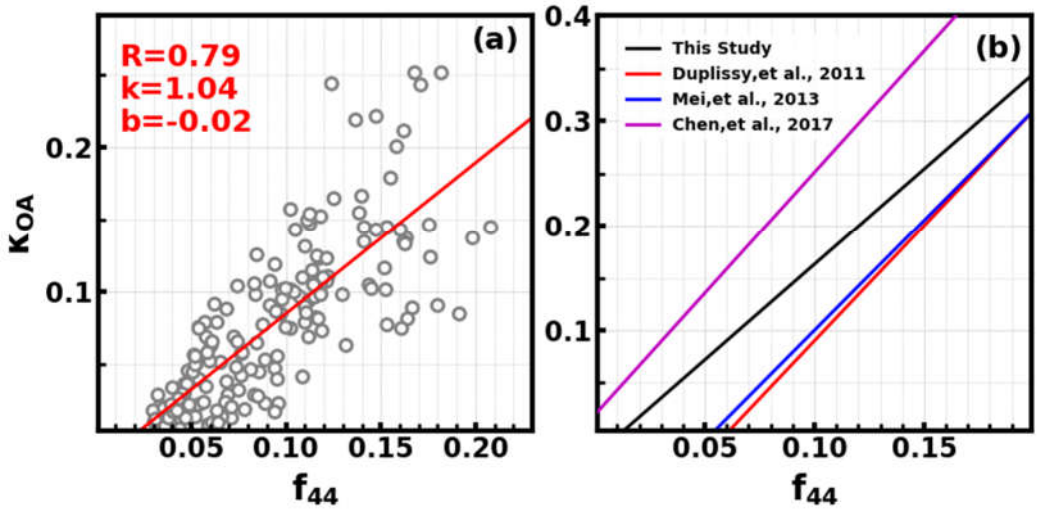

Figure 7. (a) the relationship between derived κ_{Org} and f_{44}; (b) Comparison with previous studies.

0.08 ± 0.06. This indicates that using a constant κ_{OA} value in the calculation of κ_{chem} would result in a large bias. To further investigate the impact of OA oxidation level on κ_{OA}, we compared the derived κ_{OA} against f_{44}, which is often used to represent the oxidation level of OA. Results show a clear positive correlation (R=0.79) and a statistical relationship of $\kappa_{OA} = 1.04 \cdot f_{44}$ - 0.02 (Fig.7a), indicating that the degree of oxidation level is a crucial parameter determining the OA hygroscopicity. Based on the relationship between f_{44} and O/C ratio for CV-ACSM (Hu et al., 2018b), O:C=3.47× f_{44}+0.01, the relationship between κ_{OA} and O:C can be expressed as κ_{OA}=0.3×O:C -

0.02. The derived empirical relationship between κ_{OA} and f_{44} was compared to results in previous studies (Fig.7b). As mentioned in Sect.2.3, f_{44} from CV-ToF-ACSM measurements is much higher than those previously reported from AMS, but they are well correlated and the ratio between f_{44} of CV-ToF-ACSM and previous AMS instruments for ambient aerosol ranges from 1.5 to 2 with an average of 1.75. Therefore, to be consistent with the f_{44} in previous studies, the empirical relationship in Fig.7b is changed to $\kappa_{OA} = 1.79 \cdot f_{44} - 0.03$. The κ_{OA} values are lower than that from the scheme of Chen et al. (2017), but higher than those in Duplissy et al. (2011) and Mei et al. (2013a). In general, results of most published studies about κ_{OA} demonstrate that hygroscopicity of organic aerosol generally increases as the oxidation level of organic aerosol increases, however, the empirical mathematical relationship differs much among different studies (Hong et al., 2018). These results highlight that more studies are required to study the influence of OA oxidation level on κ_{OA} and to derive a more universal parameterization scheme that can be used in chemical transport models.

4.3 Distinct diurnal variations of κ_{OA} and its relationship with OOA

The time series of derived κ_{OA} are depicted in Fig.8a, which showed large fluctuations in a day. The average κ_{OA} (Fig.8b) displays a distinct diurnal variation, with κ_{OA} reaching its minimum (0.02) in the morning (near 07:30 LT) and increasing quickly to a maximum (0.19) near 14:30 LT. As a consequence, the water uptake abilities of organic aerosol particles changed from nearly hydrophobic to moderately hygroscopic within 7 hours during daytime. Although previous results from observations in Japan also revealed significant κ_{OA} diurnal variations, however, with daily minima in the afternoon hours due to the increase of less oxygenated OA mass fractions (Deng et al. (2018) and Deng et al. (2019))，such large variability and significant diurnal variations of κ_{OA} were observed for the first time on the NCP. We found that the diurnal profile of the mass fraction OOA in OA (f_{OOA}) was remarkably similar to that of κ_{OA} (R=0.8, Figs. 8a and 8c), suggesting that OOA is very likely the determining factor of κ_{OA} in winter on the NCP.

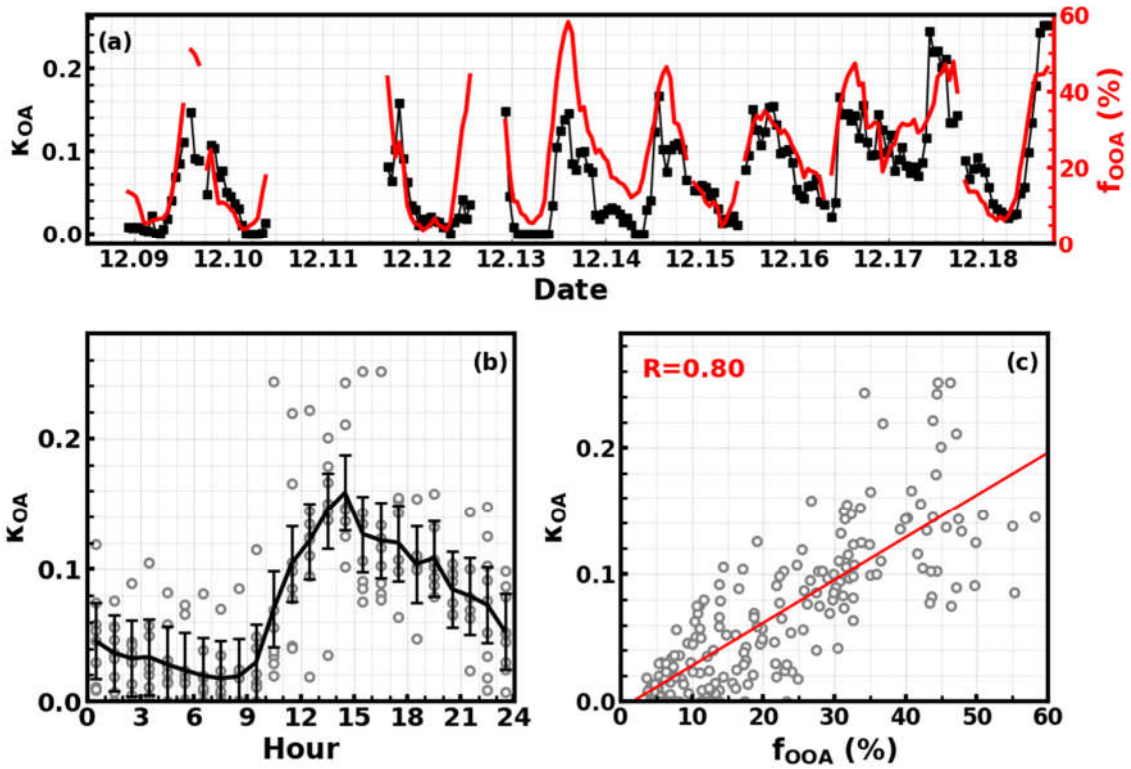

Figure 8. (a) Time series of derived κ_{Org} and OOA mass fraction in NR-PM_1 (f_{OOA}) in the right y-axis; (b) Average diurnal profile of κ_{Org}; (c) Scatter points of κ_{Org} versus f_{OOA} (%), and red line is the fitting line with linear regression.

544

545 The correlation coefficient between the average diurnal profiles of κ_{OA} and f_{OOA} was 0.95,
546 which suggests that the variations in f_{OOA} was driving the significant diurnal variations of κ_{OA}. The
547 average diurnal variations of mass concentrations of identified OOA, HOA, COA, CCOA, BBOA, and
548 their mass fractions in total organic mass are shown in Fig.9a and Fig.9b, respectively. The mass
549 concentrations of HOA, CCOA and BBOA decreased rapidly from the morning time to 15:00 LT due
550 to the rising boundary layer height and also the decreased primary source emissions. The mass
551 concentrations of COA increased a little in the morning and then decreased quickly after 09:30 LT.
552 This transitory increase of COA in the morning might be associated with the cooking for breakfast.
553 However, the OOA mass increased rapidly from about 07:30 to 10:30 LT despite the boundary layer

development during period of time , and then remained almost constant thereafter. The rapid decreases in primary organic aerosol components and the increases in OOA concentration together resulted in a dramatic increase of f_{OOA} from ~10% at 9:00 to ~45% at 13:30 LT in the afternoon, which also

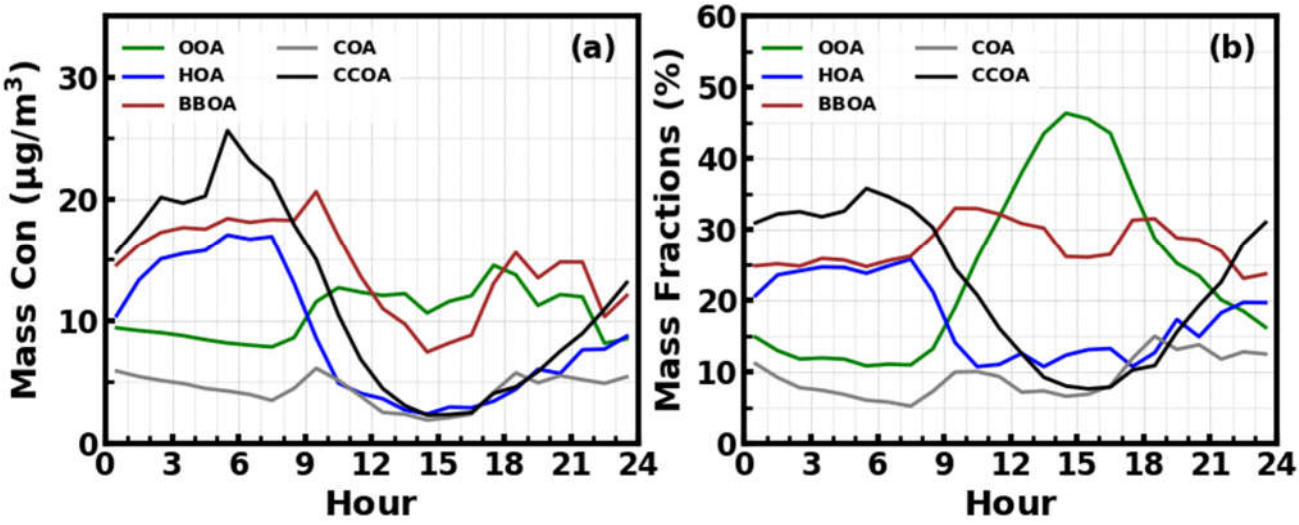

Figure 9. (a) Average diurnal profiles of mass concentrations of OOA, HOA, COA, CCOA, BBOA; (b) Average diurnal variations of mass fractions of OOA, HOA, COA, CCOA, BBOA.

corresponds to the similar increase in κ_{OA}. After 14:30 LT, the OOA mass concentration remained relatively unchanged, however, of the large increases in primary organic aerosol components also led to considerable decreases in f_{OOA} and κ_{OA}.

5 Conclusions

A field campaign was conducted at a rural site on the North China Plain in winter 2018.The major instruments deployed were a humidified nephelometer system and a CV-ToF-ACSM for the measurements of the bulk aerosol hygroscopicity of PM_{10} and PM_1 and bulk aerosol chemical compositions of $PM_{2.5}$ and PM_1. The measured σ_{sp} at 525 nm of PM_1 and PM_{10} in dry state ranged from 11 to 1875 Mm^{-1} and from 18 to 2732 Mm^{-1} with average values of 550 and 814 Mm^{-1}, respectively, suggesting a relatively polluted environment during this stusy. Retrieved $\kappa_{f(\mathrm{RH})}$ of PM_{10} and PM_1 ranged from 0.02 to 0.27, and from 0.03 to 0.26, with averages of 0.12 and 0.12, respectively. The difference of $\kappa_{f(\mathrm{RH})}$ between PM_{10} and PM_1 was found to be relatively small (3.5% on average), which was consistent with the physical and mathematical interpretation of $\kappa_{f(\mathrm{RH})}$.

A method for estimating κ_{OA} (organic aerosol hygroscopicity) base on $f(\mathrm{RH})$ and bulk aerosol chemical composition measurements is developed. The key part of this method is that the size cut of

bulk aerosol chemical composition measurements should be PM_1 no matter the bulk $\kappa_{f(RH)}$ is retrieved from light scattering enhancement measurements of PM_1 or PM_{10}. The derived κ_{OA} ranged from 0.0 to 0.25 with an average of 0.08, highlighting that κ_{OA} displayed a large variability on the NCP. Therefore, using a constant κ_{OA} could introduce a considerable uncertainty. in evaluating the climatic and environmental effects of organic aerosols The variation of κ_{OA} was highly and positively correlated with the oxidation degree of OA, and κ_{OA} showed a distinct diurnal variation with the minimum in the morning (0.02) and maximum in the afternoon (0.16). These results indicated the rapid changes in hygroscopic properties of OA in a day by evolving from nearly hydrophobic to moderately hygroscopic within 7 hours. The distinct diurnal variations of κ_{OA} were strongly associated with the changes in f_{OOA}, suggesting that the rapid formation of OOA together with of the decreases in primary organic aerosol during daytime together resulted in and the changes in κ_{OA}.

The large variability and distinct diurnal variations in κ_{OA} found in this study highlight an urgent need for more studies on the spatial and temporal variations of κ_{OA} on the NCP region, and also a better parameterization of κ_{OA} in chemical transport models to evaluate the impacts of OA on radiative forcing and CCN.

Data availability. The data used in this study are available from the corresponding author upon request (kuangye@jnu.edu.cn) and (sunyele@mail.iap.ac.cn).

Competing interests. The authors declare that they have no conflict of interest.

Author Contributions. YK conceived and organized this paper. YC, HS, NM, YK and JT planned this campaign. YK, YS and NM designed the experiments. YK and YH conducted the ACSM and aerosol light scattering enhancement factor measurements. YZ and SZ conducted the particle number size distribution measurements. JS and WY conducted the black carbon measurements. YH performed the ACSM PMF analysis. WX, YH, YS, CZ, PZ and YC helped the data analysis, and WX helped much in the language editing. YK, YH and YS prepared the manuscript with contributions from all co-authors.

Acknowledgments

This work is supported by National Key Research and Development Program of China (Grant 2017YFC0210104)，National Natural Science Foundation of China (91644218), the National research program for key issues in air pollution control (DQGG0103), This work is supported by the National Natural Science Foundation of China (41805109) and the Guangdong Innovative and Entrepreneurial Research Team Program (Research team on atmospheric environmental roles and effects of carbonaceous species: 2016ZT06N263). We also thanks scientists and technicians from Max Planck Institute for Chemistry, Mainz for supporting this field campaign.

References

Bergin, M. H., Cass, G. R., Xu, J., Fang, C., Zeng, L. M., Yu, T., Salmon, L. G., Kiang, C. S., Tang, X. Y., Zhang, Y. H., and Chameides, W. L.: Aerosol radiative, physical, and chemical properties in Beijing during June 1999, J. Geophys. Res.-Atmos., 106, 17969-17980, 10.1029/2001jd900073, 2001.

Bian, Y. X., Zhao, C. S., Ma, N., Chen, J., and Xu, W. Y.: A study of aerosol liquid water content based on hygroscopicity measurements at high relative humidity in the North China Plain, Atmos. Chem. Phys., 14, 6417-6426, 10.5194/acp-14-6417-2014, 2014.

Bougiatioti, A., Bezantakos, S., Stavroulas, I., Kalivitis, N., Kokkalis, P., Biskos, G., Mihalopoulos, N., Papayannis, A., and Nenes, A.: Biomass-burning impact on CCN number, hygroscopicity and cloud formation during summertime in the eastern Mediterranean, Atmos. Chem. Phys., 16, 7389-7409, 10.5194/acp-16-7389-2016, 2016.

Brock, C. A., Wagner, N. L., Anderson, B. E., Attwood, A. R., Beyersdorf, A., Campuzano-Jost, P., Carlton, A. G., Day, D. A., Diskin, G. S., Gordon, T. D., Jimenez, J. L., Lack, D. A., Liao, J., Markovic, M. Z., Middlebrook, A. M., Ng, N. L., Perring, A. E., Richardson, M. S., Schwarz, J. P., Washenfelder, R. A., Welti, A., Xu, L., Ziemba, L. D., and Murphy, D. M.: Aerosol optical properties in the southeastern United States in summer – Part 1: Hygroscopic growth, Atmospheric Chemistry and Physics, 16, 4987-5007, 10.5194/acp-16-4987-2016, 2016.

Cerully, K. M., Bougiatioti, A., Hite Jr, J. R., Guo, H., Xu, L., Ng, N. L., Weber, R., and Nenes, A.: On the link between hygroscopicity, volatility, and oxidation state of ambient and water-soluble aerosols in the southeastern United States, Atmos. Chem. Phys., 15, 8679-8694, 10.5194/acp-15-8679-2015, 2015.

Chang, R. Y. W., Slowik, J. G., Shantz, N. C., Vlasenko, A., Liggio, J., Sjostedt, S. J., Leaitch, W. R., and Abbatt, J. P. D.: The hygroscopicity parameter (κ) of ambient organic aerosol at a field site subject to biogenic and anthropogenic influences: relationship to degree of aerosol oxidation, Atmos. Chem. Phys., 10, 5047-5064, 10.5194/acp-10-5047-2010, 2010.

Chen, J., Zhao, C. S., Ma, N., and Yan, P.: Aerosol hygroscopicity parameter derived from the light scattering enhancement factor measurements in the North China Plain, Atmos. Chem. Phys. Discuss., 14, 3459-3497, 10.5194/acpd-14-3459-2014, 2014.

Chen, J., Budisulistiorini, S. H., Itoh, M., Lee, W. C., Miyakawa, T., Komazaki, Y., Yang, L. D. Q., and Kuwata, M.: Water uptake by fresh Indonesian peat burning particles is limited by water-soluble organic matter, Atmos. Chem. Phys., 17, 11591-11604, 10.5194/acp-17-11591-2017, 2017.

Cheng, Y. F., Wiedensohler, A., Eichler, H., Su, H., Gnauk, T., Brueggemann, E., Herrmann, H., Heintzenberg, J., Slanina, J., Tuch, T., Hu, M., and Zhang, Y. H.: Aerosol optical properties and related chemical apportionment at Xinken in Pearl River Delta of China, Atmospheric Environment, 42, 6351-6372, 10.1016/j.atmosenv.2008.02.034, 2008.

Deng, Y., Kagami, S., Ogawa, S., Kawana, K., Nakayama, T., Kubodera, R., Adachi, K., Hussein, T., Miyazaki, Y., and Mochida, M.: Hygroscopicity of Organic Aerosols and Their Contributions to CCN Concentrations Over a Midlatitude Forest in Japan, Journal of Geophysical Research: Atmospheres, 123, 9703-9723, 10.1029/2017jd027292, 2018.

Deng, Y., Yai, H., Fujinari, H., Kawana, K., Nakayama, T., and Mochida, M.: Diurnal variation and size dependence of the hygroscopicity of organic aerosol at a forest site in Wakayama, Japan: their relationship to CCN concentrations, Atmos. Chem. Phys., 19, 5889-5903, 10.5194/acp-19-5889-2019, 2019.

Drinovec, L., Močnik, G., Zotter, P., Prévôt, A. S. H., Ruckstuhl, C., Coz, E., Rupakheti, M., Sciare, J., Müller, T., Wiedensohler, A., and Hansen, A. D. A.: The "dual-spot" Aethalometer: an improved measurement of aerosol black carbon with real-time loading compensation, Atmospheric Measurement Techniques, 8, 1965-1979, 10.5194/amt-8-1965-2015, 2015.

Duplissy, J., DeCarlo, P. F., Dommen, J., Alfarra, M. R., Metzger, A., Barmpadimos, I., Prevot, A. S. H., Weingartner, E., Tritscher, T., Gysel, M., Aiken, A. C., Jimenez, J. L., Canagaratna, M. R., Worsnop, D. R., Collins, D. R., Tomlinson, J., and Baltensperger, U.: Relating hygroscopicity and composition of organic aerosol particulate matter, Atmos. Chem. Phys., 11, 1155-1165, 10.5194/acp-11-1155-2011, 2011.

Fröhlich, R., Cubison, M. J., Slowik, J. G., Bukowiecki, N., Prévôt, A. S. H., Baltensperger, U., Schneider, J., Kimmel, J. R., Gonin, M., Rohner, U., Worsnop, D. R., and Jayne, J. T.: The ToF-ACSM: a portable aerosol chemical speciation monitor with TOFMS detection, Atmos. Meas. Tech., 6, 3225-3241, 10.5194/amt-6-3225-2013, 2013.

Frosch, M., Bilde, M., DeCarlo, P. F., Jurányi, Z., Tritscher, T., Dommen, J., Donahue, N. M., Gysel, M., Weingartner, E., and Baltensperger, U.: Relating cloud condensation nuclei activity and oxidation level of α-pinene secondary organic aerosols, Journal of Geophysical Research: Atmospheres, 116, 10.1029/2011jd016401, 2011.

Gysel, M., Crosier, J., Topping, D. O., Whitehead, J. D., Bower, K. N., Cubison, M. J., Williams, P. I., Flynn, M. J., McFiggans, G. B., and Coe, H.: Closure study between chemical composition and hygroscopic growth of aerosol particles during TORCH2, Atmos. Chem. Phys., 7, 6131-6144, 10.5194/acp-7-6131-2007, 2007.

Hong, J., Kim, J., Nieminen, T., Duplissy, J., Ehn, M., Äijälä, M., Hao, L. Q., Nie, W., Sarnela, N., Prisle, N. L., Kulmala, M., Virtanen, A., Petäjä, T., and Kerminen, V. M.: Relating the hygroscopic properties of submicron aerosol to both gas- and particle-phase chemical composition in a boreal forest environment, Atmos. Chem. Phys., 15, 11999-12009, 10.5194/acp-15-11999-2015, 2015.

Hong, J., Xu, H., Tan, H., Yin, C., Hao, L., Li, F., Cai, M., Deng, X., Wang, N., Su, H., Cheng, Y., Wang, L., Petäjä, T., and Kerminen, V. M.: Mixing state and particle hygroscopicity of organic-dominated aerosols over the Pearl River Delta region in China, Atmos. Chem. Phys., 18, 14079-14094, 10.5194/acp-18-14079-2018, 2018.

Hu, W., Campuzano-Jost, P., Day, D. A., Croteau, P., Canagaratna, M. R., Jayne, J. T., Worsnop, D. R., and Jimenez, J. L.: Evaluation of the new capture vapourizer for aerosol mass spectrometers (AMS) through laboratory studies of inorganic species, Atmos. Meas. Tech., 10, 2897-2921, 10.5194/amt-10-2897-2017, 2017.

Hu, W., Day, D. A., Campuzano-Jost, P., Nault, B. A., Park, T., Lee, T., Croteau, P., Canagaratna, M. R., Jayne, J. T., Worsnop, D. R., and Jimenez, J. L.: Evaluation of the new capture vaporizer for aerosol mass spectrometers: Characterization of organic aerosol mass spectra, Aerosol Science and Technology, 52, 725-739, 10.1080/02786826.2018.1454584, 2018a.

Hu, W., Day, D. A., Campuzano-Jost, P., Nault, B. A., Park, T., Lee, T., Croteau, P., Canagaratna, M. R., Jayne, J. T., Worsnop, D. R., and Jimenez, J. L.: Evaluation of the New Capture Vaporizer for Aerosol Mass Spectrometers (AMS): Elemental Composition and Source Apportionment of Organic Aerosols (OA), ACS Earth and Space Chemistry, 2, 410-421,

682 10.1021/acsearthspacechem.8b00002, 2018b.
683 Jimenez, J. L., Canagaratna, M. R., Donahue, N. M., Prevot, A. S. H., Zhang, Q., Kroll, J. H., DeCarlo, P. F., Allan, J. D., Coe,
684 H., Ng, N. L., Aiken, A. C., Docherty, K. S., Ulbrich, I. M., Grieshop, A. P., Robinson, A. L., Duplissy, J., Smith, J. D., Wilson, K.
685 R., Lanz, V. A., Hueglin, C., Sun, Y. L., Tian, J., Laaksonen, A., Raatikainen, T., Rautiainen, J., Vaattovaara, P., Ehn, M., Kulmala,
686 M., Tomlinson, J. M., Collins, D. R., Cubison, M. J., Dunlea, J., Huffman, J. A., Onasch, T. B., Alfarra, M. R., Williams, P. I.,
687 Bower, K., Kondo, Y., Schneider, J., Drewnick, F., Borrmann, S., Weimer, S., Demerjian, K., Salcedo, D., Cottrell, L., Griffin,
688 R., Takami, A., Miyoshi, T., Hatakeyama, S., Shimono, A., Sun, J. Y., Zhang, Y. M., Dzepina, K., Kimmel, J. R., Sueper, D., Jayne,
689 J. T., Herndon, S. C., Trimborn, A. M., Williams, L. R., Wood, E. C., Middlebrook, A. M., Kolb, C. E., Baltensperger, U., and
690 Worsnop, D. R.: Evolution of Organic Aerosols in the Atmosphere, Science, 326, 1525-1529, 10.1126/science.1180353,
691 2009.
692 Kawana, K., Nakayama, T., and Mochida, M.: Hygroscopicity and CCN activity of atmospheric aerosol particles and their
693 relation to organics: Characteristics of urban aerosols in Nagoya, Japan, Journal of Geophysical Research: Atmospheres,
694 121, 4100-4121, 10.1002/2015JD023213, 2016.
695 Koehler, K. A., Kreidenweis, S. M., DeMott, P. J., Petters, M. D., Prenni, A. J., and Carrico, C. M.: Hygroscopicity and cloud
696 droplet activation of mineral dust aerosol, Geophysical Research Letters, 36, 10.1029/2009GL037348, 2009.
697 Kuang, Y., Zhao, C., Tao, J., Bian, Y., Ma, N., and Zhao, G.: A novel method for deriving the aerosol hygroscopicity parameter
698 based only on measurements from a humidified nephelometer system, Atmos. Chem. Phys., 17, 6651-6662, 10.5194/acp-
699 17-6651-2017, 2017.
700 Kuang, Y., Zhao, C. S., Zhao, G., Tao, J. C., Xu, W., Ma, N., and Bian, Y. X.: A novel method for calculating ambient aerosol
701 liquid water content based on measurements of a humidified nephelometer system, Atmospheric Measurement
702 Techniques, 11, 2967-2982, 10.5194/amt-11-2967-2018, 2018.
703 Lambe, A. T., Onasch, T. B., Massoli, P., Croasdale, D. R., Wright, J. P., Ahern, A. T., Williams, L. R., Worsnop, D. R., Brune,
704 W. H., and Davidovits, P.: Laboratory studies of the chemical composition and cloud condensation nuclei (CCN) activity of
705 secondary organic aerosol (SOA) and oxidized primary organic aerosol (OPOA), Atmos. Chem. Phys., 11, 8913-8928,
706 10.5194/acp-11-8913-2011, 2011.
707 Li, X., Song, S., Zhou, W., Hao, J., Worsnop, D. R., and Jiang, J.: Interactions between aerosol organic components and liquid
708 water content during haze episodes in Beijing, Atmos. Chem. Phys. Discuss., 2019, 1-19, 10.5194/acp-2019-316, 2019.
709 Liu, H. J., Zhao, C. S., Nekat, B., Ma, N., Wiedensohler, A., van Pinxteren, D., Spindler, G., Müller, K., and Herrmann, H.:
710 Aerosol hygroscopicity derived from size-segregated chemical composition and its parameterization in the North China
711 Plain, Atmos. Chem. Phys., 14, 2525-2539, 10.5194/acp-14-2525-2014, 2014.
712 Liu, X., and Wang, J.: How important is organic aerosol hygroscopicity to aerosol indirect forcing?, Environmental Research
713 Letters, 5, 044010, 10.1088/1748-9326/5/4/044010, 2010.
714 Ma, N., Zhao, C. S., Nowak, A., Müller, T., Pfeifer, S., Cheng, Y. F., Deng, Z. Z., Liu, P. F., Xu, W. Y., Ran, L., Yan, P., Göbel, T.,
715 Hallbauer, E., Mildenberger, K., Henning, S., Yu, J., Chen, L. L., Zhou, X. J., Stratmann, F., and Wiedensohler, A.: Aerosol
716 optical properties in the North China Plain during HaChi campaign: an in-situ optical closure study, Atmos. Chem. Phys.,
717 11, 5959-5973, 10.5194/acp-11-5959-2011, 2011.
718 Massoli, P., Lambe, A. T., Ahern, A. T., Williams, L. R., Ehn, M., Mikkilä, J., Canagaratna, M. R., Brune, W. H., Onasch, T. B.,
719 Jayne, J. T., Petäjä, T., Kulmala, M., Laaksonen, A., Kolb, C. E., Davidovits, P., and Worsnop, D. R.: Relationship between
720 aerosol oxidation level and hygroscopic properties of laboratory generated secondary organic aerosol (SOA) particles,
721 Geophysical Research Letters, 37, 10.1029/2010gl045258, 2010.
722 Mei, F., Hayes, P. L., Ortega, A., Taylor, J. W., Allan, J. D., Gilman, J., Kuster, W., de Gouw, J., Jimenez, J. L., and Wang, J.:
723 Droplet activation properties of organic aerosols observed at an urban site during CalNex-LA, Journal of Geophysical
724 Research: Atmospheres, 118, 2903-2917, 10.1002/jgrd.50285, 2013a.
725 Mei, F., Setyan, A., Zhang, Q., and Wang, J.: CCN activity of organic aerosols observed downwind of urban emissions during

CARES, Atmos. Chem. Phys., 13, 12155-12169, 10.5194/acp-13-12155-2013, 2013b.
Paatero, P., and Tapper, U.: Positive matrix factorization: A non-negative factor model with optimal utilization of error estimates of data values, Environmetrics, 5, 111-126, 10.1002/env.3170050203, 1994.
Petters, M. D., and Kreidenweis, S. M.: A single parameter representation of hygroscopic growth and cloud condensation nucleus activity, Atmospheric Chemistry and Physics, 7, 1961-1971, 2007.
Quinn, P. K., Coffman, D. J., Bates, T. S., Miller, T. L., Johnson, J. E., Welton, E. J., Neusüss, C., Miller, M., and Sheridan, P. J.: Aerosol optical properties during INDOEX 1999: Means, variability, and controlling factors, Journal of Geophysical Research: Atmospheres, 107, INX2 19-11-INX12 19-25, 10.1029/2000jd000037, 2002.
Rastak, N., Pajunoja, A., Acosta Navarro, J. C., Ma, J., Song, M., Partridge, D. G., Kirkevåg, A., Leong, Y., Hu, W. W., Taylor, N. F., Lambe, A., Cerully, K., Bougiatioti, A., Liu, P., Krejci, R., Petäjä, T., Percival, C., Davidovits, P., Worsnop, D. R., Ekman, A. M. L., Nenes, A., Martin, S., Jimenez, J. L., Collins, D. R., Topping, D. O., Bertram, A. K., Zuend, A., Virtanen, A., and Riipinen, I.: Microphysical explanation of the RH-dependent water affinity of biogenic organic aerosol and its importance for climate, Geophysical Research Letters, 44, 5167-5177, 10.1002/2017gl073056, 2017.
Rose, D., Nowak, A., Achtert, P., Wiedensohler, A., Hu, M., Shao, M., Zhang, Y., Andreae, M. O., and Pöschl, U.: Cloud condensation nuclei in polluted air and biomass burning smoke near the mega-city Guangzhou, China – Part 1: Size-resolved measurements and implications for the modeling of aerosol particle hygroscopicity and CCN activity, Atmos. Chem. Phys., 10, 3365-3383, 10.5194/acp-10-3365-2010, 2010.
Shao, L., Li, W., Yang, S., Shi, Z., and Lü, S.: Mineralogical characteristics of airborne particles collected in Beijing during a severe Asian dust storm period in spring 2002, Science in China Series D: Earth Sciences $V 50, 953-959, 2007.
Sherman, J. P., Sheridan, P. J., Ogren, J. A., Andrews, E., Hageman, D., Schmeisser, L., Jefferson, A., and Sharma, S.: A multi-year study of lower tropospheric aerosol variability and systematic relationships from four North American regions, Atmos. Chem. Phys., 15, 12487-12517, 10.5194/acp-15-12487-2015, 2015.
Thalman, R., de Sá, S. S., Palm, B. B., Barbosa, H. M. J., Pöhlker, M. L., Alexander, M. L., Brito, J., Carbone, S., Castillo, P., Day, D. A., Kuang, C., Manzi, A., Ng, N. L., Sedlacek Iii, A. J., Souza, R., Springston, S., Watson, T., Pöhlker, C., Pöschl, U., Andreae, M. O., Artaxo, P., Jimenez, J. L., Martin, S. T., and Wang, J.: CCN activity and organic hygroscopicity of aerosols downwind of an urban region in central Amazonia: seasonal and diel variations and impact of anthropogenic emissions, Atmospheric Chemistry and Physics, 17, 11779-11801, 10.5194/acp-17-11779-2017, 2017.
Titos, G., Cazorla, A., Zieger, P., Andrews, E., Lyamani, H., Granados-Muñoz, M. J., Olmo, F. J., and Alados-Arboledas, L.: Effect of hygroscopic growth on the aerosol light-scattering coefficient: A review of measurements, techniques and error sources, Atmospheric Environment, 141, 494-507, https://doi.org/10.1016/j.atmosenv.2016.07.021, 2016.
Ulbrich, I. M., Canagaratna, M. R., Zhang, Q., Worsnop, D. R., and Jimenez, J. L.: Interpretation of organic components from Positive Matrix Factorization of aerosol mass spectrometric data, Atmos. Chem. Phys., 9, 2891-2918, 10.5194/acp-9-2891-2009, 2009.
Wiedensohler, A., Birmili, W., Nowak, A., Sonntag, A., Weinhold, K., Merkel, M., Wehner, B., Tuch, T., Pfeifer, S., Fiebig, M., Fjäraa, A. M., Asmi, E., Sellegri, K., Depuy, R., Venzac, H., Villani, P., Laj, P., Aalto, P., Ogren, J. A., Swietlicki, E., Williams, P., Roldin, P., Quincey, P., Hüglin, C., Fierz-Schmidhauser, R., Gysel, M., Weingartner, E., Riccobono, F., Santos, S., Grüning, C., Faloon, K., Beddows, D., Harrison, R., Monahan, C., Jennings, S. G., O'Dowd, C. D., Marinoni, A., Horn, H. G., Keck, L., Jiang, J., Scheckman, J., McMurry, P. H., Deng, Z., Zhao, C. S., Moerman, M., Henzing, B., de Leeuw, G., Löschau, G., and Bastian, S.: Mobility particle size spectrometers: harmonization of technical standards and data structure to facilitate high quality long-term observations of atmospheric particle number size distributions, Atmos. Meas. Tech., 5, 657-685, 10.5194/amt-5-657-2012, 2012.
Williams, B. J., Goldstein, A. H., Kreisberg, N. M., Hering, S. V., Worsnop, D. R., Ulbrich, I. M., Docherty, K. S., and Jimenez, J. L.: Major components of atmospheric organic aerosol in southern California as determined by hourly measurements of source marker compounds, Atmos. Chem. Phys., 10, 11577-11603, 10.5194/acp-10-11577-2010, 2010.

Wu, Z. J., Poulain, L., Henning, S., Dieckmann, K., Birmili, W., Merkel, M., van Pinxteren, D., Spindler, G., Müller, K., Stratmann, F., Herrmann, H., and Wiedensohler, A.: Relating particle hygroscopicity and CCN activity to chemical composition during the HCCT-2010 field campaign, Atmos. Chem. Phys., 13, 7983-7996, 10.5194/acp-13-7983-2013, 2013.

Wu, Z. J., Zheng, J., Shang, D. J., Du, Z. F., Wu, Y. S., Zeng, L. M., Wiedensohler, A., and Hu, M.: Particle hygroscopicity and its link to chemical composition in the urban atmosphere of Beijing, China, during summertime, Atmos. Chem. Phys., 16, 1123-1138, 10.5194/acp-16-1123-2016, 2016.

Xu, W., Croteau, P., Williams, L., Canagaratna, M., Onasch, T., Cross, E., Zhang, X., Robinson, W., Worsnop, D., and Jayne, J.: Laboratory characterization of an aerosol chemical speciation monitor with PM2.5 measurement capability, Aerosol Science and Technology, 51, 69-83, 10.1080/02786826.2016.1241859, 2017.

Zhang, F., Li, Y., Li, Z., Sun, L., Li, R., Zhao, C., Wang, P., Sun, Y., Liu, X., Li, J., Li, P., Ren, G., and Fan, T.: Aerosol hygroscopicity and cloud condensation nuclei activity during the AC3Exp campaign: implications for cloud condensation nuclei parameterization, Atmos. Chem. Phys., 14, 13423-13437, 10.5194/acp-14-13423-2014, 2014.

Zhang, Q., Jimenez, J. L., Canagaratna, M. R., Ulbrich, I. M., Ng, N. L., Worsnop, D. R., and Sun, Y.: Understanding atmospheric organic aerosols via factor analysis of aerosol mass spectrometry: a review, Analytical and Bioanalytical Chemistry, 401, 3045-3067, 10.1007/s00216-011-5355-y, 2011.